CAPITAL UNIVERSITY OF SCIENCE AND TECHNOLOGY, ISLAMABAD

Mixed Convection Nanofluid Flow with Inclined Magnetic Field and Joule Heating Effects over Porous Backward Facing Step

by

Madiha Iqbal

A thesis submitted in partial fulfillment for the degree of Master of Philosophy

in the

Faculty of Computing
Department of Mathematics

2020

This thesis is dedicated to my beloved mother, **Shaheen Iqbal** who always stood by my side whenever I wanted to do something positive, to my father, **Mohammad Iqbal** whose support always lifted me up and finally to **Dr. Shafqat Hussain** whose valuable instructions and expertise gave me courage in difficult times.

CERTIFICATE OF APPROVAL

Mixed Convection Nanofluid Flow with Inclined Magnetic Field and Joule Heating Effects over Porous Backward Facing Step

by

Madiha Iqbal

(MMT173032)

THESIS EXAMINING COMMITTEE

S. No.	Examiner	Name	Organization
(a)	External Examiner	Dr. Tanveer Akbar Kayani	COMSATS University, Islamabad
(b)	Internal Examiner	Dr. Mohammad Afzal	CUST, Islamabad
(c)	Supervisor	Dr. Shafqat Hussain	CUST, Islamabad

Dr. Shafqat Hussain
Thesis Supervisor
May, 2020

Dr. Muhammad Sagheer
Head
Dept. of Mathematics
May, 2020

Dr. Muhammad Abdul Qadir
Dean
Faculty of Computing
May, 2020

Author's Declaration

I, **Madiha Iqbal** hereby state that my MS thesis titled "**Mixed Convection Nanofluid Flow with Inclined Magnetic Field and Joule Heating Effects over Porous Backward Facing Step**" is my own work and has not been submitted previously by me for taking any degree from Capital University of Science and Technology, Islamabad or anywhere else in the country/abroad.

At any time if my statement is found to be incorrect even after my graduation, the University has the right to withdraw my M. Phill Degree.

Madiha Iqbal

(MMT173032)

Plagiarism Undertaking

I solemnly declare that research work presented in this thesis titled "*Mixed Convection Nanofluid Flow with Inclined Magnetic Field . . .*" is solely my research work with no significant contribution from any other person. Small contribution/help wherever taken has been dully acknowledged and that complete thesis has been written by me.

I understand the zero tolerance policy of the HEC and Capital University of Science and Technology towards plagiarism. Therefore, I as an author of the above titled thesis declare that no portion of my thesis has been plagiarized and any material used as reference is properly referred/cited.

I undertake that if I am found guilty of any formal plagiarism in the above titled thesis even after award of MPhill degree, the University reserves the right to withdraw/revoke my MPhill degree and that HEC and the University have the right to publish my name on the HEC/University website on which names of students are placed who submitted plagiarized work.

Madiha Iqbal

(MMT173032)

Acknowledgements

First of all I must say Alhmdulillah to pay gratitude to **ALLAH** who made my ways easy to achieve my goal and who is always Great, even if His creation praise Him or not. He knows what and when it's best for us. Also, the **Prophet Muhammad (Peace Be Upon Him)** who is a guidance in every aspect of life for the betterment of Humanity.

I am fortunate Alhmdulillah and would like to say a special thanks to my supervisor **Dr. Shafqat Hussain**, Associate Professor in Capital University of Science and Technology, for not only letting me explore this problem but also helping me at every step in the research and my thesis compilation.

Madiha Iqbal

(MMT173032)

Abstract

The present investigation is based on a numerical study of laminar mixed convection of nanofluid flow over a porous backward facing step with varying inclination of magnetic field and Joule heating effect. The bottom wall of the channel downstream of the step is maintained at isothermal heating and the other walls of the channel are assumed to be adiabatic. Governing equations are solved by finite element method. Velocity components and temperature are discretized by the biquadratic finite element space. Pressure is discretized using linear discontinuous finite element space. The discretized non linear equations are linearized by using fixed point iteration scheme. Corresponding linear problem is solved by the Gaussian elimination method. The effects of Reynolds number, Hartmann number, orientation angle of the magnetic field and solid volume fraction of the nanofluid on the fluid flow in a backward facing step geometry has been examined. Moreover, the results are shown by isotherms and streamlines. Also, some useful MATLAB graphs are drawn to yield results. It has been observed from the results that average heat transfer has been declined for increasing Da values. An increment in average Nusselt number has been noticed for increases Reynolds number, ϵ the porosity parameter as well as for the inclination angle γ of the magnetic field.

Contents

List of Figures

List of Tables

Abbreviations

BDF	Darcy-Brinkman-Forchheimer
BFS	Backward Facing Step
FEM	Finite Element Method
LBB	Ladyzhenskaya-Babuska-Brezzi
MHD	Magnetohydrodynamics
PDEs	Partial Differential Equations

Symbols

c_p	specific heat constant ($J\ kg^{-1}\ K^{-1}$)
$\mathbf{g}$	gravitational acceleration ($m\ s^{-2}$)
k	thermal conductivity ($kgm\ s^3\ K^{-1}$)
Nu	local Nusselt number
Nu_{avg}	averaged Nusselt number
Nu_l	Local Nusselt number
Pr	Prandtl number ($\frac{\nu_f}{\alpha_f}$)
Ri	Richardson number ($\frac{GR}{Re^2}$)
Ha	Hartmann number ($B_0 L\sqrt{\sigma_f/\mu_{nf}}$)
Ec	Eckert number $\left(\frac{U_L^2}{C_p(T_h-T_c)}\right)$
Re	Reynolds number ($\frac{UL}{\nu}$)
Gr	Grashof number, ($\frac{g\beta\rho^2 L^3\Delta T}{\mu^2}$)
Da	Darcy number (K/L^2)
$\mathbf{B}$	External magnetic field strength ($N\ m\ s^{-1}$)
K	Permeability of porous medium (m^2)
T	fluid temperature (K)
T_h	hot lower wall temperature (K)
T_c	cold upper moving wall temperature (K)
ΔT	temperature gradient (K)
T_∞	is bulk temperature (K)
p	dimensional pressure
P	non-dimensional pressure
u	dimensional velocity in x-direction ($m\ s^{-1}$)

U	dimensionless velocity component in x-direction
v	dimensional velocity in y-direction ($m\ s^{-1}$)
V	dimensionless velocity component in y-direction
u_0	inlet flow velocity
$\mathbf{U}$	standard flow velocity

Greek symbols

α	thermal diffusivity ($m^2\ s^{-1}$)
β	thermal expansion coefficient (K^{-1})
ϕ	volume fraction of nanoparticles
θ	non-dimensional temperature $\left(\frac{T-T_c}{T_h-T_c}\right)$
ρ	density ($kg\ m^{-3}$)
σ	electrical conductivity
μ	dynamic viscosity ($kg\ m^{-1}\ s^{-1}$)
ν	kinematic viscosity ($m^2\ s^{-1}$)
ϵ	Porosity of medium
γ	Magnetic field inclination
κ	Thermal conductivity ($kg\ m\ s^3\ K^{-1}$)
$\tau^\star$	Viscous stresses on flow ($N\ m^{-2}$)
Φ	Viscous dissipation

Subscripts

avg	average
c	cold
h	hot
f	base fluid
nf	nanofluid
p	nanoparticles

Chapter 1

Introduction

The present research investigates the impact of magnetic field inclination and porosity on the mixed convection of nanofluid flow over a backward facing step. Because of the importance of backward and forward facing step in engineering and industry it has drawn the attention of many researchers [1]. Early studies on this benchmark problem were made in 1950's. Flow separation studies were on its peak in twentieth century and can be seen typically around the wings of aeroplanes, pipes, turbines and air around the skyscrapers and tall buildings [2] where they come across sudden expansions. Backward facing step is one of the examples where such expansions are commonly seen. Further details regarding the backward facing step are discussed as follows.

1.1 Backward Facing Step

Geometry of the backward facing step is simple yet it exhibits complex flow behaviour. Flow separation is not the only feature, there are many other flow behaviours to study for practical purposes for example eddies, wakes, vortices, reverse flows, recirculation regions and reattachment of the flow etc. "The horizontal distance between the step and the reattachment point is defined as the reattachment length" [3]. The work has been investigated for this benchmark problem is both

on laminar and turbulent models [3, 4]. Early works have been carried out using transformations with geometry and fundamental flow behaviour whereas advancement in numerical and computational areas was touched in 1980's [5]. The work on 2D configurations having horizontal, vertical and inclined backward-facing step was investigated by several researchers who reached at the conclusion that the effects of buoyancy forces on heat transfer is less in horizontal and more in vertical and inclined cases. Moreover, in case of the 2D horizonal backward-facing step with air circulation having uniform wall temperature revealed that Nu does not depend upon Re and with the increasing buoyancy force, recirculation region and Nu decreased [6]. Attributes for flow and heat transfer for backward facing step were studied by Iwai et al. [7] at low Re to explore the aspect ratio of the channel. Many heat exchanging device configurations, for example condensers, evaporators, boilers and backward facing step are similar in the sense that they have immediate expansions in their geometry. Both 2D and 3D studies have been carried out in this geometry. In 3D heat exchanging devices where all of the surrounding walls are heated, Nie and Armaly [8] studied 3D flow for wall temperature distributions, Nu and other important parameters for laminar convection flow adjacent to backward facing step in a rectangular duct. A helpful data for design optimization was obtained from this study. Armaly et al. [9] inquired experimentally and theoretically the flow over backward facing step using Laser Doppler measurements for velocity reattachment length, showing extra regions of flow separation which was not found in earlier literature.

1.2 Nanofluids

Nanoparticles hold equal importance in material science, medicine, physics and many more which has made it a cynosure of present century. The shape, size and surface area of naoparticles have given them a non-typical transport and heat transfer behaviour which cannot be explained by traditional theories. When a large particle is broken down into several particles, surface area of these particles is enhanced many times than the large particle this is the reason due to which

they are high in mobility and efficiency [10, 11]. It is being broadly used from food packaging to storage capacity of microprocessors and from automobile industry to air conditioning. This journey was started by Richard Feynman, a nobel prize winner who for the very first time gave the idea of micro-machines in 1959. Then in 1974, the term 'Nanotechnology' was introduced. First time the term 'nanofluid' was used by Choi [12] and he victoriously produced nanofluids in 1995. Most of the research work was considered between the year 2010 and 2012 [13]. There is a wide variety of nanoparticles which are categorised according to their shape, size, conductivity, both thermal and electrical and heat transfer abilities. They are generally made up of metals, carbides or oxides [14]. Some are named as nanofibers, nanowires, nanotubes, nanosheet and nanorods or droplets. The research on enhancing thermal conductivity of fluids like water, air and oil also known as host fluid, has been taking place for the last hundred years by adding metallic or nonmetallic guest particles. These particles include Copper (Cu), Silver (Ag), Alumina (Al_2O_3), Titanium oxide (TiO_2) and Zinc Oxide (ZnO) etc, and base fluid can be ethylene glycol, oil, engine oil and water etc. A large number of literature is dedicated to heat transportation of nanofluids under convection [15]. Preparation methods of nanofluids are two-phase, single-phase and other novel methods. However its sedimentation and stability are among the major issues. First one is widely being used in industry and is economical but unstable. Yu and Xie [16] addressed the issue of instability of nanofluids. They proposed the techniques and implementation for the preparation of nanofluids that are stable.

1.2.1 Nanofluids in Backward Facing Step

Because of the extensive use of heat exchange devices in engineering such as nuclear reactors, car radiators, air heating and cooling applications, regaining of heat loss and refrigerators, researchers have put lot of efforts to amplify rate of heat transfer. Thermal conductivity of the fluids without nanoarticles was limited which was improved after pouring calculated volume fractions into it [17]. Significance of

nanofluids becomes higher when studied with backward-forward steping. According to Selimefendigil and Öztop [18], the problem arises when reattachment and separation of fluid are encountered together. Numerical simulation was performed for mixed convection nanofluid past over backward facing step with a revolving cylinder as an obstacle. Effects of various parameters along with cylinder's angular velocity and volume fraction of the nanofluid were studied. Backward facing with nanofluids for heat transfer magnification with separated flows were studied by Abu-Nada [19]. Aside from dissimilar nanofluid volume fraction, different types of nanoparticles were used as well. It was noticed that out of the recirculation zone, Nu was increased on using nanoparticles with high thermal ability and vice versa for those with low thermal ability, within the recirculation region.

1.2.2 Heat Transfer in Nanofluids

The research in convective heat transfer through nanofluids has been conducted from the last few decades. Heat transfer trough convection directly depends upon the boundary condition of the geometry, fluid's thermal conductivity and it is also explored to be increased by adding suspended particles [20]. Suggestions for possible causes of heat transfer in nanofluids were given by Trisaksria and Wongwises [21]. Fast heat transfer ability of nanofluids has been used in solar collectors and solar heating of water. These devices absorb sunlight in the form of radiations and transfer it to the fluid running through the solar panels for water heating which can be stored for further use [22]. Impact and heat transfer of TiO nanoparticles in water with natural convection was studied by Wen and Ding [23]. Nanofluids were formulated by electrostatic stabilization and high shear mixing. The adopted way for nanofluids formulation was highly stable and their thermal trend was studied too. This review disclose that the application of the nanofluids for heat transfer increment does not depend upon thermal conductivity only but also upon other parameters like their size, shape and dispersion. Thermal conductivity of nanofluids can be determined by mostly used transient hot wire

method [24]. As nanofluids are electrically conducting too that is why an alterative method was proposed for appropriate measurement [25].

1.3 Mixed Convection

Convection can be grouped into three types, natural or free convection, forced convection and mixed convection. Free convection is one in which fluid motion is due to the density differences produced by the temperature differences within the fluid. If the fluid motion is produced with the help of "a pump, a blower or some similar device, the process is called forced convection". When both are involved that is the "mixed convection" [26]. Computer advancement in memory and speed have helped us to do numerical study with precision. With the help of which we can add more discretization points and solve more complex problems. Many industrial procedures and natural circumstances do involve heat transfer either by force or free convection such as heating and cooling phenomena, electrical appliances, microprocessor cooling and solar collectors [27]. Heat transfer by mixed convection in a horizonal chamber with openings in foot and top walls was numerically studied considering nanofluid of Al_2O_3-water [28]. Affects of Re and ϕ on fluid flow and heat transfer were examined. It explored satisfactory increase in heat transfer and temperature due to increase in ϕ while fluid flow and temperature distribution showed dependency upon Re.

1.3.1 Mixed Convection in Backward Facing Step

Steady mixed convective flow over 3D steping is studied by Saldana [29]. A comparison between mixed and pure forced convection with differences between velocity and temperature distribution was numerically simulated. Abu-Mulaweh [30] provided a deep scrutiny on single-phase mixed convective flow and transport of heat within the fluid in both forward and backward steping at several unlike angles. Many of previously estimated inter depending variable quantities were reproduced

by making some assumption and changing important parameters. Thermal behavior of nanofluids' pulsating flow with forced convection over backward facing step with a immobile cylinder was studied by Selimefendigil and Öztop [31]. Consequences of parameters like frequency, Re and ϕ on the flow and heat transfer features were investigated numerically. Enhanced oscillation frequency, Re and ϕ resulted in enhancement of heat transfer. Reduced order model is an attribute grounded on database of fluids and structural models. It helps in reduction of computational cost yet satisfactory precision. A revolving cylinder exposed to nanofluid over BFS with mixed convection was studied [18] for reduced order model. The impact of several parameters upon heat transfer was studied. An increment in heat transfer was seen on blend of specific parameters. Forced convection features with laminar flow over 2D backward stepping with circular cylinder was considered by Kumar and Dhiman [32].

1.4 Magnetohydrodynamics

Magnetohydrodynamics or MHD in short, also known by magnetofluid mechanics or hydromagnetics, is a study of fluids that conduct electricity under a magnetic field. In this way the fluid which is already electrically conducting passes through magnetic field, induces current. This action produces forces on the fluid which has effects back on magnetic field. Hannes Alfvén [33] in 1970, won Nobel Prize for giving first time the idea of MHD. Examples of such fluids are plasmas, salt water, liquid form of metals, or electrolytes. It effects flow of electrically conducting fluid. When a conducting fluid moves through a magnetic field, it induces current, as a result Lorentz force is produced which changes the movement of the fluid. The important fields related to MHD are solar physics, plasma physics, cooling in fission reaction and experiments in laboratory plasma. Physical laws of the flow are obtained from the laws of fluid dynamics and Maxwell's equations.

Magnetic field has effects on the temperature distribution and heat transfer on the fluid flow. A numerical inspection in square 2D cavity for the effects of magnetic field over flow and heat transfer was conducted by Bakar et al. [34]. Changes in

Nu along with streamlines patters and isotherm were observed. The laminar flow of a viscous incompressible fluid conducting electricity over a backward steping was inspected numerically under the MHD theory with $Re = 380$ and Stuart number N scaling $0 \leq N \leq 0.2$ by Abbassi and Nassrallah [35]. Heat transfer was measured against Pr equals 0.02 for liquid metal and Pr equals 7 for water. Measuring the length of reattachment revealed that external magnetic field made recirculation zone to decrease. From the velocity behavior it was shown that the induced magnetic force damped the fundamental flow out of the recirculation region and flow near boundaries moved more quickly. Moreover, magnetic field notably increased heat transfer for elevated values of Pr. Numerical inspection of nanofluids with laminar forced convection over a backward steping through a channel held by Al-aswadi et al. [6] by applying FVM. Several nanoparticles like Al_2O_3, CuO, diamond and SiO_2 were used with $\phi = 5\%$ in the base fluid. Step height and expansion ratio were taken to be $4.8mm$ and $2mm$ respectively with Re ranging from 50 to 175. Nanoparticles of SiO_2 were reported to have the maximum velocity as compared to other particle types, while nanoparticles of Ag has the minimum velocity. Initially a recirculation zone was reported after the step started and flow became fully developed afterwards. Also, reattachment point moved opposite to upstream and away from the step point as Re is elevated.

1.5 Mixed Convection Heat Transfer of Nanofluids in Backward Facing Step

Two dimensional laminar flow with mixed convection over a straight plane microscale backward stepig placed in channel was numerically inquired by Kherbeet at el. [36]. Several nanoparticles types were used to conduct the experiment. The Nu was notised to be increased with increasing values of Re and nanofluid volume fraction which was highest with particles of Silicon dioxide (SiO_2). Again Kherbeet at el. [37] performed experiment for laminar nanofluids above microscale backward facing step to check the consequences upon heat transfer attributes. Beside the

step height, Re and taking some parameters in consideration, it was found that Nu was greatest with SiO_2 and with MFFS (microscale backward-facing step) as compared to MBFS (microscale forward-facing step). Heat transfer and fluid flow properties over a backward or forward steping trough duct with obstacles is worked upon by fewer researchers. A square obstacle positioned before the step in pulsating laminar flow above a backward steping with varying Pr, Re and positions of obstacle were numerically investigated by Selimefendigil [38]. It was reported that obstacle position can be used as the key to handle heat transfer. Laminar nanofluids flow over backward steping under forced convection was mathematically inquired [39]. The foot wall of the step was elastic. Flexibility of the wall effected the flow of the fluid and heat transfer. When Re and ϕ were increased, local and averaged heat transfer elevated. At highest Re, the heat transfer was highest with less elasticity of foot wall.

1.6 Porous Medium in Backward Facing Step

Applications of porous media spread over vast fields. It is significant for energy and transport properties. In the nature, exemplary models are underground water flows, flow of drugs in tissues [40], oil flow in reservoirs [41] and subsoil heat flow [42]. In industry foamy materials, detergent pellets, textiles and food drying [42] are included. Therefore, it is crucial to understand their shrinking, swelling, absorbing behavior and flow of fluids through them for their extensive use in modelling scientific and engineering problems. Khanafer and Chamkha [43] simulated a study with porous medium upon Brinkman-extended Darcy model. They inspected that Nu_{avg} enhances on increasing Darcy number. Hassan and Ismael [44] investigated in the lid driven cavity by using Maxwell Brinkman model. They explored that augmentation of average heat transfer is achieved by reduction in Da value.

Backward facing step or geometries with separated flow phenomena and reattachment come across several industrial, engineering and electronic devices. These include turbine blade cooling, combustion chamber cooling, sedimentation and

bed formation in rivers and cooing in nuclear reactors, etc [29]. Another aspect is that inducing this coupled flow phenomena helps to achieve conditions and flow behaviour favourable for heat transfer. Researchers are continuously analyzing the behaviour experimentally and numerically. After the literature survey, it has seemingly shown that the present configuration with introduction of porous medium and Joule's heating has not been investigated yet. The main incentive of the present research work is to study this important flow geometry and corresponding controlling parameters which are significantly and directly related to the cooling or heating in BFS.

1.7 Thesis Contribution

The objective of the present work is to review the numerical examination of magnetic field impact upon mixed convection nanofluids with laminar flow above backward facing step(BFS) and to extend this configuration for porous medium and Joule heating effects due to viscous dissipation. The Governing PDEs are non dimensionalized through appropriate transformation parameters. Non dimensionalized PDEs are solved with the help of Galerkin weighted residual method based on finite element method. Particularly, the finite element Q_2/P_1^{disc} that satisfies the LLB-stability condition, has been used to discretize the non dimensionalized model. Bi-quadratic, Q_2 is used for temperature and components of velocity whereas, P_1^{disc} as a linear element is used for pressure components. The contribution of magnetic field is added to the x and y-momentum equations. Viscous dissipation due to magnetic field is added to the energy equation in the form of Joule heating. Effects of governing parameters upon fluid flow and heat transfer over BFS configuration were inspected numerically. Numerical work has been presented with the help of streamlines, isotherms and MATLAB graphs.

1.8 Thesis Attributes

This thesis is further comprised of the following four chapters:

In **Chapter 2**, fundamental laws along with conceptual definitions are provided. Non dimensionalized parameters are defined in the chapter. An overview of solution methodology is also given. parameters

In **Chapter 3**, influence of inclined magnetic field on mixed convective nanofluid over backward facing step has been considered. The proposed problem with associated boundary conditions is provided and dimensional form of the physical model is non dimensionalized by introducing non dimensional parameters. The continuous form of non dimensional equations is converted into discrete form with Q_2/P_1^{disc} element. The discretized non linear algebraic equations are linearized by the fixed point iteration and Gaussian elimination is adopted to solve the corresponding linear system. The convergence of the solution is achieved by taking Euclidean norm of the residual. Produced results are interpreted numerically and presented using streamlines and isotherms. MATLAB graphs are also produced to show the solution results.

Chapter 4 extends the study of [1] reviewed in **Chapter 3** will be extended by introducing porosity and effects of Joule heating in the forgoing problem. Non linear coupled PDEs are discretized with Galerkin weighted residual based FEM discretization. Impact of parameters Re, Ha, Da, Ec, γ, ϕ and ϵ over heat transfer, was studied through graphs, streamlines and isotherms.

Chapter 5 provides conclusive summary of the thesis.

Chapter 2

Fundamental Concepts and Basic Equations of Flow

Some relevant definitions and basic concept to the fluid are described below. Dimensionless physical quantities and fundamental equations of flow along with the solution methodology to be adopted, are also mentioned in this chapter.

2.1 Important Definitions

Definition 2.1.1. (**Fluid**)

"A substance in the liquid or gas phase is referred to as a fluid. A fluid deforms continuously under the influence of a shear stress, no matter how small" [45]. There are several examples of fluids from daily life usage. These are breathing, blood flow [46], honey, the movement of people on the platform of a railway station, air flowing across the wings of a jet, starch solution, oil and water e.t.c. Fluid comprises of the states of matter and include gases, liquids and plasma [47].

Definition 2.1.2. (**Fluid Mechanics**) [48]

"The fluid mechanics is defined as the science that deals with the behavior of fluids at rest (fluid statics) or in motion (fluid dynamics)".

Branches of Fluid Mechanics:

Definition 2.1.3. (**Fluid Dynamics**) [48]

"The branch that deals with bodies in motion is called Fluid Dynamics".

Definition 2.1.4. (**Fluid Statics**) [48]

"The branch of mechanics that deals with bodies at rest is called statics".

Definition 2.1.5. (**Nanofluid**) [49]

"Nanofluids are engineered by suspending nanoparticles with average sizes below 100 nm in traditional heat transfer fluids such as water, oil, and ethylene glycol. A very small amount of guest nanoparticles, when dispersed uniformly and suspended stably in host fluids, can provide dramatic improvements in the thermal properties of host fluids".

Definition 2.1.6. (**Viscosity**) [48]

"There is a property that represents the internal resistance of a fluid to motion or the fluidity and that property is the viscosity".

Definition 2.1.7. (**Kinematic Viscosity**) [48]

"The ratio of dynamic viscosity to density appears frequently. For convenience, this ratio is given the name kinematic viscosity ν and is expressed as"

$$\nu = \frac{\mu}{\rho} \tag{2.1}$$

Definition 2.1.8. (**Dynamic Viscosity**) [48]

"Viscosity is a property of a fluid that quantifies the ratio of shear stress to rate of deformation (strain rate) of a fluid particle", can be expressed by

$$\mu = \frac{\text{shear stress}}{\text{strain rate}}, \tag{2.2}$$

"The terms absolute viscosity, dynamic viscosity, and viscosity are synonymous"

Definition 2.1.9. (**Strain Rate**) [48]

"Strain rate can also be called deformation rate. This is the rate at which a fluid particle deforms (i.e., changes shape) at a given position and time in a fluid flow".

2.2 Types of Fluids

Definition 2.2.1. (**Ideal Fluid vs Real Fluid**)
"Ideal fluid is fluid which has no viscosity and it is also incompressible. There is no fluid in nature which fully behaves as ideal fluid". It is also assumed that such fluid "has negligible viscous effects". Practically no ideal fluid exists. While fluids that continuously deform under viscosity and are compressible too are known to be real fluid".

Definition 2.2.2. (**Newtonian Fluid vs non-Newtonian Fluid**) [48]
"Fluids for which the rate of deformation is linearly proportional to the shear stress are called Newtonian fluids. In one-dimensional shear flow of Newtonian fluids, shear stress can be expressed by the linear relationship as

$$\text{Shear stress} := \tau = \mu \frac{du}{dy}, \tag{2.3}$$

where the constant of proportionality μ is called the coefficient of viscosity or the dynamic (or absolute) viscosity of the fluid". Examples are air, water, kerosene and gasoline. "Fluids for which the shear stress is not linearly related to the shear strain rate are called non-Newtonian fluids. Examples include slurries and colloidal suspensions, polymer solutions, blood, paste, and cake batter".

Definition 2.2.3. (**Compressible vs Incompressible Flow**) [48]
"Flows that involve significant changes in density. Such flows are called compressible flows". Mathematically,

$$\rho \neq \text{constant}$$

"A fluid flow where variations in density are sufficiently small to be negligible. Flows are generally incompressible".

$$\rho = \text{constant}$$

"Any characteristic of a system is called a property. Some familiar properties are pressure P, temperature T, volume v, and mass m".

Definition 2.2.4. (**Density**) [48]

"Density is defined as the mass per unit volume". That is,

$$\text{Density}: \qquad \rho = \frac{m}{v} \tag{2.4}$$

Definition 2.2.5. (**Stress**) [48]

"Stress is defined as force per unit area and is determined by dividing the force by the area upon which it acts". It has two components, normal and tangential.

Components of Stress:

Definition 2.2.6. (**Normal Stress**) [48]

"The normal component of a force acting on a surface per unit area is called the normal stress".

$$\text{Normal stress: } \sigma = F_n/dA$$

Definition 2.2.7. (**Shear Stress**) [48]

"Tangential component of a force acting on a surface per unit area is called shear stress".

$$\text{Shear stress: } \tau = F_t/dA$$

Definition 2.2.8. (**Pressure**) [48]

"In a fluid at rest, the normal stress is called pressure. A fluid at rest is at a state of zero shear stress".

$$P = \tfrac{F}{A}$$

Definition 2.2.9. (**Magnetohydrodynamics**) [50]

"Magnetohydrodynamics is the multi-disciplinary study of the flow of electrically conducting fluids in electromagnetic fields. Examples of such fluids include plasmas, liquid metals and salt water".

2.3 Types of Flow

Definition 2.3.1. (**External vs Internal Flow**) [48]

"The flow of an unbounded fluid over a surface such as a plate, a wire, or a pipe is

external flow. The flow in a pipe or duct is internal flow if the fluid is completely bounded by solid surfaces". For example, flow of water in a pipe is internal flow.

Definition 2.3.2. (**Laminar vs Turbulent Flow**) [51]
"Laminar flow is a flow which takes place in layers. There is no mixing of fluid particles between any two adjacent layers. The flow will be laminar when velocity of flow is low". While a turbulent flow is one "when the velocity of flow reaches a certain limit such that the fluid particles no longer move in layers or laminae. Violent mixing of fluid particles takes place due to which they move in random manner". As a result velocity varies both in magnitude and direction from instant to instant.

Definition 2.3.3. (**Steady vs Unsteady Flow**) [48]
"The term steady implies no change of properties, velocity, temperature, etc., at a point with time. The opposite of steady is unsteady".

Definition 2.3.4. (**Uniform vs Non-Uniform Flow**)
"A flow, in which the fluid particles possess equal velocities at each section of the channel or pipe is called uniform" [52]. Mathematically,

$$\left(\frac{\partial \mathbf{U}}{\partial \mathbf{s}}\right) = \begin{pmatrix} \frac{\partial u}{\partial s} \\ \frac{\partial v}{\partial s} \\ \frac{\partial \omega}{\partial s} \end{pmatrix} = 0,$$

while a non-uniform flow is one for which this is not true [51].

$$\left(\frac{\partial \mathbf{U}}{\partial \mathbf{s}}\right) = \begin{pmatrix} \frac{\partial u}{\partial s} \\ \frac{\partial v}{\partial s} \\ \frac{\partial \omega}{\partial s} \end{pmatrix} \neq 0$$

Definition 2.3.5. (**Natural vs Forced Flow**) [48]
"A fluid flow is said to be natural or forced, depending on how the fluid motion is initiated. In forced flow, a fluid is forced to flow over a surface or in a pipe by external means" for example by a pump or a fan. Whereas "in natural flows, fluid motion is due to natural means such as the buoyancy effect".

2.4 Modes of Heat Transfer

"Conduction, convection and radiation are the three modes of heat transfer" [53].

Definition 2.4.1. (**Conduction**) [26]
"Conduction is the transfer of heat from one part of a body at a higher temperature to another part of the same body at a lower temperature".

Definition 2.4.2. (**Convection**) [26]
"Convection, relates to the transfer of heat from a bounding surface to a fluid in motion, or to the heat transfer across a flow plane within the interior of the flowing fluid".

Definition 2.4.3. (**Forced Convection**) [26]
"If the fluid motion is induced by a pump, a blower, a fan, or some similar device, the process is called forced convection".

Definition 2.4.4. (**Natural Convection**) [26]
"If the fluid motion occurs as a result of the density difference produced by the temperature difference, the process is called free or natural convection".

Definition 2.4.5. (**Mixed Convection**) [26]
"Mixed convection occurs when both natural convection and forced convection play significant roles in the transfer of heat. Mixed convection occurs when the heat transfer is significantly different from that for either pure natural convection or pure forced convection".

Definition 2.4.6. (**Radiation**) [26]
"Radiation, or more correctly thermal radiation, is electromagnetic radiation emitted by a body by virtue of its temperature and at the expense of its internal energy". Examples are visible light, x rays, and radio waves. "All heated solids and liquids, as well as some gases, emit thermal radiation. The transfer of energy by conduction requires the presence of a material medium, while radiation does not".

2.5 Dimensionless Parametres

Definition 2.5.1. (**Nusselt Number**)(German engineer, Wilhelm (1882–1957)) [54]

"Important parameter in convective heat transfer is the heat transfer coefficient, defined by Newton's law of cooling. To present more generalized results, this quantity is non dimensionalized and called the Nusselt number, defined as,

$$Nu = hL/k$$

where L is a characteristic dimension, h is heat transfer coefficient and k is the thermal conductivity of the fluid" [54]. "It expresses the ratio of the total heat transfer by convection in a system to the heat transfer by conduction", i.e. "Convection heat transfer/conduction heat transfer" [48].

Definition 2.5.2. (**Reynolds Number**)(British engineer, Osborne Reynolds (1842–1912)) [54]

"The most important parameter in fluid mechanics". It is always important in all heat transfer modes. It can be expressed as: "Inertia/Viscosity" [55].
Defined by "the ratio of the inertial term over the viscous force term" [47]. It tells the flow character either laminar, turbulent or transient [54]. Mathematically,

$$Re = UL/\nu,$$

Definition 2.5.3. (**Richardson Number**)(English mathematician, Lewis Fry Richardson (1881-1953)) [54]

"This number expresses the potential-to-kinetic energies ratio" [54]. Also, defined by: "Buoyancy force/Inertial force" [48].

$$Ri = \frac{g\beta L\Delta T\rho^2}{\mu^2}, \tag{2.5}$$

$$Ri = \frac{Gr}{Re^2}. \tag{2.6}$$

Definition 2.5.4. (**Prandtl Number**)

It's importance is in Heat Convection. This can also be expressed as "dissipation/-conduction" [48]. "This number expresses the ratio of the momentum diffusivity (viscosity) to the thermal diffusivity. It characterizes the physical properties of a

fluid with convective and diffusive heat transfers" [54].

Mathematically,

$$Pr = \frac{\nu}{\alpha}, \tag{2.7}$$

where, ν is momentum or kinetic diffusivity and α is thermal diffusivity.

$Pr << 1$ heat transfer by conduction is dominated.

$Pr = 1$ heat transfer by both conduction and convection.

$Pr >> 1$ heat transfer by convection is dominated [54].

Definition 2.5.5. (**Hartmann Number**)(Danish physicist, George Poul Hartmann (1881-1951)) [54]

"It is an important criterion of magneto-hydrodynamics. It expresses the ratio of the induced electrodynamic (magnetic) force to the hydrodynamic force of the viscosity".

$$Ha = B_0 L \sqrt{\frac{\sigma_f}{\mu_f}}$$

where, B_0 is magnetic field strength and L is characteristic length dimension.

Definition 2.5.6. (**Grashof Number**) [54](German engineer, Franz Grashof (1826–1893))

"A dimensionless parameter, important in natural convection heat transfer of fluids, is the Grashof number [55].

$$Gr = \frac{g\beta\rho^2 L^3 \Delta T}{\mu^2}, \tag{2.8}$$

where g is the acceleration of gravity, β is the thermal expansion coefficient, ρ the density, L characteristic length, ΔT a temperature difference, and μ the viscosity".

Definition 2.5.7. (**Eckert Number**) [54](American engineer, Georg Eckert (1904-2004))

"It expresses the ratio of kinetic energy to the thermal energy change".

Mathematically,

$$Ec = \frac{U^2}{c_p \Delta T} \tag{2.9}$$

Here, ΔT is "temperature difference".

Definition 2.5.8. (**Darcy Number**) [54](Gaspard Darcy)
"It characterizes the permeability in porous material".
Mathematically,

$$Da = \frac{K}{L^2}, \tag{2.10}$$

where, "K" is the "permeability of porous material".

2.6 Fundamental Flow Equations

"The conservation relations are also called balance equations since any conserved quantity must balance during a process" [48].

2.6.1 Continuity Equation

"Conservation of mass, often called the continuity relation, states that the fluid mass cannot change [46]". Mathematical form of the relation is,

$$\frac{\partial \rho}{\partial t} + \nabla \cdot (\rho \mathbf{U}) = 0 \tag{2.11}$$

where, ρ is the density.
For steady fluid flow, above equation becomes

$$\nabla \cdot (\rho \mathbf{U}) = 0 \tag{2.12}$$

Furthermore, if the flow is incompressible, then

$$\nabla \cdot \mathbf{U} = 0 \tag{2.13}$$

2.6.2 Conservation of Momentum

"Newton's second law states that the rate of change of momentum of a fluid particle equals the sum of the forces on the particle" [53]. i.e., "Rate of increase of momentum of fluid particle = Sum of forces on fluid particle". Momentum conservation principle is based on the Newton's second law which says that "The momentum of a system remains constant when the net force acting on it is zero and thus the momentum of such systems is conserved. This is known as the conservation of momentum principle" [48]. The forces acting on the fluid are divided into two types, surface and body forces. Prior includes forces of pressure and viscous force and latter are force of gravity, Centrifugal, Coriolis and electromagnetic forces. The Momentum conservation principle is stated as:

$$\frac{\partial \rho \mathbf{U}}{\partial t} = -(\nabla . \rho \mathbf{U})\mathbf{U} - \nabla P + \nabla . \tau_{ij}^{\star} + \rho \mathbf{g}. \tag{2.14}$$

After the contribution of continuity equation, above equation becomes

$$\rho \frac{D\mathbf{U}}{Dt} = -\nabla P + \nabla . \tau_{ij}^{\star} + \rho \mathbf{g}. \tag{2.15}$$

This equation is Newton's second law of motion. Momentum conservation principle is based on Newton's second law that states that "the rate of change of the momentum of a body is equal to the net force acting on the body" [48]. In the above equation, ρ is density, $\mathbf{U}$ is the fluid velocity, P is pressure, $\mathbf{g}$ is gravitational force and τ_{ij}^{*} is viscous stress tensor given by:

$$\tau_{ij}^{\star} = \begin{pmatrix} \tau_{xx} & \tau_{yx} & \tau_{zx} \\ \tau_{xy} & \tau_{yy} & \tau_{zy} \\ \tau_{xz} & \tau_{yz} & \tau_{zz} \end{pmatrix}, \tag{2.16}$$

or

$$\tau_{ij}^{\star} = \begin{pmatrix} \sigma_{xx} & \tau_{yx} & \tau_{zx} \\ \tau_{xy} & \sigma_{yy} & \tau_{zy} \\ \tau_{xz} & \tau_{yz} & \sigma_{zz} \end{pmatrix}. \tag{2.17}$$

Ideal fluids for which $\mu = 0$, the Eq. (2.15) takes the form

$$\rho \frac{D\mathbf{U}}{Dt} = -\nabla P + \rho \mathbf{g}, \tag{2.18}$$

is well known Euler's equation of motion.

After incorporating the nine components of viscous stress tensor $\tau_{ij}^{\star}$ into the Eq. (2.15), we have the famous Navier-Stokes equations for Newtonian, incompressible fluids with constant density and μ, given as follows:

For this, first we write the vector form of the Eq. (2.15) in component form:

$$\rho \frac{\partial u}{\partial t} = -\frac{\partial p}{\partial x} + \frac{\partial \tau_{xx}}{\partial x} + \frac{\partial \tau_{yx}}{\partial y} + \frac{\partial \tau_{zx}}{\partial z} + \rho g_x, \tag{2.19}$$

$$\rho \frac{\partial v}{\partial t} = -\frac{\partial p}{\partial y} + \frac{\partial \tau_{xy}}{\partial x} + \frac{\partial \tau_{yy}}{\partial y} + \frac{\partial \tau_{zy}}{\partial z} + \rho g_y, \tag{2.20}$$

$$\rho \frac{\partial w}{\partial t} = -\frac{\partial p}{\partial z} + \frac{\partial \tau_{xz}}{\partial x} + \frac{\partial \tau_{yz}}{\partial y} + \frac{\partial \tau_{zz}}{\partial z} + \rho g_z, \tag{2.21}$$

where, $\mathbf{U} = (u, v, w)$ and $\mathbf{g} = (g_x, g_y, g_z)$ The values of nine components are:

$$\tau_{ij}^{*} = \begin{pmatrix} 2\mu\frac{\partial u}{\partial x} & \mu(\frac{\partial v}{\partial x} + \frac{\partial u}{\partial y}) & \mu(\frac{\partial w}{\partial x} + \frac{\partial u}{\partial z}) \\ \mu(\frac{\partial u}{\partial y} + \frac{\partial v}{\partial x}) & 2\mu\frac{\partial v}{\partial y} & \mu(\frac{\partial w}{\partial y} + \frac{\partial v}{\partial z}) \\ \mu(\frac{\partial u}{\partial z} + \frac{\partial w}{\partial x}) & \mu(\frac{\partial v}{\partial z} + \frac{\partial w}{\partial y}) & 2\mu\frac{\partial w}{\partial z} \end{pmatrix}. \tag{2.22}$$

After the substitution, the Eqs. (2.19) - (2.6.2) become,

$$\rho \frac{\partial u}{\partial t} = -\frac{\partial p}{\partial x} + \mu \left(\frac{\partial^2 u}{\partial x^2} + \frac{\partial^2 u}{\partial y^2} + \frac{\partial^2 u}{\partial z^2} \right) + \rho g_x, \tag{2.23}$$

$$\rho \frac{\partial v}{\partial t} = -\frac{\partial p}{\partial y} + \mu \left(\frac{\partial^2 v}{\partial x^2} + \frac{\partial^2 v}{\partial y^2} + \frac{\partial^2 v}{\partial z^2} \right) + \rho g_y, \tag{2.24}$$

$$\rho \frac{\partial w}{\partial t} = -\frac{\partial p}{\partial z} + \mu \left(\frac{\partial^2 w}{\partial x^2} + \frac{\partial^2 w}{\partial y^2} + \frac{\partial^2 w}{\partial z^2} \right) + \rho g_z. \tag{2.25}$$

The vector form of Navier-Stokes equation is [26]:

$$\rho \frac{D\mathbf{U}}{Dt} = -\nabla p + \mu \Delta \mathbf{U} + \rho \mathbf{g} \tag{2.26}$$

Here, D/Dt is total derivative or substantial derivative.

2.6.3 Conservation of Energy

"One of the most fundamental laws in nature is the first law of thermodynamics, also known as the conservation of energy principle. It states that energy can be neither created nor destroyed during a process; it can only change forms" [48]. "The energy equation is derived from the first law of thermodynamics, which states that the rate of change of energy of a fluid particle is equal to the rate of heat addition to the fluid particle plus the rate of work done on the particle" [53]. Mathematical form is [26]:

$$\frac{\partial}{\partial t}\rho(e+\frac{1}{2}\mathbf{U}^2) = -\nabla.\rho\mathbf{U}(e+\frac{1}{2}\mathbf{U}^2)-\nabla.\mathbf{q}^{''}+\rho(\mathbf{U}.g)-\nabla.P\mathbf{U}+\nabla.(\tau^{\star}_{ij}.\mathbf{U})+q^{'''}. \quad (2.27)$$

Here, $E = e+\frac{1}{2}\mathbf{U}^2$. E is total energy of the fluid, e is the internal energy and $\frac{1}{2}\mathbf{U}^2$ is kinetic energy while potential energy is treated separately and included in work term on R.H.S of the equation. Also, $\nabla.\mathbf{q}^{''}$ and $q^{'''}$ are conduction due to heat flux and source term, respectively. Utilizing continuity and momentum equation, Eq. (2.27) becomes,

$$\rho\frac{De}{Dt} = -P(\nabla.\mathbf{U}) - \nabla.\mathbf{q}^{''} + \nabla\mathbf{U} : \tau^{\star}_{ij} + S_e, \quad (2.28)$$

where,

$$S_e = \rho(\mathbf{U}.g) + q^{'''} \quad (2.29)$$

$$\nabla\mathbf{U} : \tau^{\star}_{ij} = \left(\sigma_x\frac{\partial u}{\partial x} + \tau^{\star}_{xy}\frac{\partial u}{\partial y} + \tau^{\star}_{xz}\frac{\partial u}{\partial z}\right) + \left(\tau^{\star}_{yx}\frac{\partial v}{\partial x} + \sigma_y\frac{\partial v}{\partial y} + \tau^{\star}_{yz}\frac{\partial v}{\partial z}\right) \quad (2.30)$$
$$+ \left(\tau^{\star}_{zx}\frac{\partial w}{\partial x} + \tau^{\star}_{zy}\frac{\partial w}{\partial y} + \sigma_z\frac{\partial w}{\partial z}\right).$$

Here, source term is further rewritten as S_e, absorbing the potential energy and body forces in it. The Eq. (2.28) can be easily achieved by multiplying x, y and

z momentum equations with u, v and w, respectively and adding them up. This equation is subtracted through the Eq. (2.27) [53]. Substituting the values from Eq. (2.22) into the Eq. (2.30), the above expression implies [26],

$$\nabla \mathbf{U} : \tau_{ij}^{\star} = \mu \Bigg[2 \left(\left(\frac{\partial u}{\partial x} \right)^2 + \left(\frac{\partial v}{\partial y} \right)^2 + \left(\frac{\partial w}{\partial z} \right)^2 \right) + \left(\frac{\partial u}{\partial y} + \frac{\partial v}{\partial x} \right)^2 + \left(\frac{\partial w}{\partial y} + \frac{\partial v}{\partial z} \right)^2 + \left(\frac{\partial u}{\partial z} + \frac{\partial w}{\partial x} \right)^2 \Bigg], \tag{2.31}$$

$$\nabla \mathbf{U} : \tau_{ij}^{\star} = \mu \Phi, \tag{2.32}$$

where, Φ is "viscous dissipation". It expresses all those impacts that are under the "viscous stresses" [53].

Using Eq. (2.32) into Eq. (2.28) and after introducing Fourier's law , we obtain

$$\rho \frac{De}{Dt} = -P(\nabla . \mathbf{U}) - \nabla . (-\kappa \nabla T) + \mu \Phi + S_e. \tag{2.33}$$

For incompressible flow, a relation $e = c_v T$ and $\nabla . \mathbf{U} = 0$ can be used. Here, c_v is "specific heat at constant volume". That gives work done under pressure force equals zero. Therefore, the equation can be written for temperature field as follows,

$$\rho c_v \frac{DT}{Dt} = \kappa \Delta T + \mu \Phi + S_e \tag{2.34}$$

where, $e = c_v T$ is the "internal energy".

$$\rho c_v \frac{DT}{Dt} = \kappa \Delta T, \tag{2.35}$$

$$\frac{DT}{Dt} = \alpha \Delta T, \tag{2.36}$$

where, $\alpha = \frac{\kappa}{\rho c_v}$ is "thermal diffusivity". The validity of this equation is under steady, viscous, incompressible Newtonian fluid flow with neglected viscous effects due to internal energy [46, 53].

2.7 Finite Element Method

Finite element method, FEM in short, is a flexible and widespread aid to solve PDEs and integro differential equations of the physical problems, in science and engineering. The advancements in the method forged ahead in 1950s and this all was possible only with the help of modern computers. It provides solutions to structural as well as non-structural problems. The method is widely used to approximate solutions to the problems for solid mechanics, structural mechanics, fluid flow, heat transfer and stress analysis etc [56]. It "involves modelling the structure using small interconnected elements called *finite elements*" [57]. With the help of FEM, continuous form of the problem is transformed into discontinuous or discrete form.

2.8 FEM Formulation

FEM can easily handle both structural and non structural grids. For the curvilinear boundaries, FEM formulation is ideal. There are three major steps involved.

1. **Discretize and Select the Element types**

   In this step the computational domain is subdivided into non-overlapping subdomains known as, finite elements [57]. For 1D, these elements join each other at points $x_1, x_2, x_3 ...., x_{n-1}$. Add $x_0 = a$ and $x_n = b$ to this array. In general we may call them as $x_i's$. The type of element is chosen so that it simulates the behaviour of the physical model the most, keeping the computational cost as low as possible.

2. **Select an Approximating Function**

   An approximating function known as basis function or interpolation polynomial $\tilde{u}(x)$ is to be selected in this step, which represents the variation of dependent variable $u(x)$ over the elements.

3. **Application of Weighted Residual Method**

   Since any of the weighted residual method can be then applied but more famous is Galerkin method which is applied to each element separately, subjected to the given differential equation between the end nodal values $\tilde{u}(x_i)$ and $\tilde{u}(x_j)$. Here $\tilde{u}(x_i)'s$ are the approximations to the true solution $u(x_i)'s$, of the given differential equation.

2.9 Galerkin Weighted Residual Method

We can apply weighted residual methods to the differential equation directly which develop the finite element equations [57]. In Galerkin's method, shape functions are chosen as weight functions. Galerkin's method gives discrete solution at discrete number of points.

$$\omega = \frac{\partial \tilde{u}}{\partial u_i} = \phi_i, (i = 1, 2, ..., n). \tag{2.37}$$

The unknowns are obtained by letting the integral of weighted residual over Ω, to be vanished. For 1D problem with domain $[a, b]$ we have,

$$\int_a^b \omega_i R dx = 0, (i = 1, 2, ..., n), \tag{2.38}$$

The linear system of equations thus obtained is,

$$\begin{bmatrix} \int_a^b \phi_1 \triangle(\phi_1) dx & \dots & \dots & \int_a^b \phi_1 \triangle(\phi_n) dx \\ \vdots & \ddots & & \vdots \\ \vdots & & \ddots & \vdots \\ \int_a^b \phi_n \triangle(\phi_1) dx & \dots & \dots & \int_a^b \phi_n \triangle(\phi_n) dx \end{bmatrix} \begin{bmatrix} u_1 \\ \vdots \\ \vdots \\ u_n \end{bmatrix} = \begin{bmatrix} \int_a^b \phi_1 f dx \\ \vdots \\ \vdots \\ \int_a^b \phi_n f dx \end{bmatrix}. \tag{2.39}$$

Chapter 3

Influence of Inclination Angle of Magnetic Field on Mixed Convective Nanofluid over Backward Facing Step

This chapter contains the numerical study of the mixed convection of nanofluid flow over a backward facing step under the influence of varying magnetic field inclination [1]. We are interested in reinvestigating the dimensionless coupled PDEs defining physical phenomena. By using required dimensionless parameters, the dimensional PDEs are changed into dimensionless form. The numerical study is being done by using FEM to discretize the continuous form of physical laws. After obtaining a weak formulation, a set of algebraic equations are obtained for numerical manipulation. To visualize the effects of different parameters, streamline, isothermal patterns and MATLAB graphs are used to illustrate it. "The reattachment length is the distance from the step at which the flow resumes in the positive flow direction all over the cross-section" [58].

3.1 Problem Formulation

A combined convection nanofluid flow under the effect of inclined magnetic field over BFS is considered. Angle of inclination of the magnetic field of strength B_0, is taken to be γ ($0° \leq \gamma \leq 90°$). The inlet fluid velocity is u_0. In the present geometry, flow is considered to be two dimensional laminar, steady state. The channel is open at both ends. The open channel is a backward facing step with step size H and height of the channel is $2H$. A schematic diagram of the geometry is shown by Figure 3.1. Inlet of the channel is maintained at a uniform temperature $T = T_c$ and possesses a parabolic velocity profile. The length of the step in downstream direction, starting from foot of the step to the outlet is, $36H$. Except the bottom wall of step which is maintained at $T = T_h$, all the other walls of the channel are set at a thermal insulation. The channel contains Cu-water nanofluid, flowing under a magnetic field influenced by an orientation. Impact of several parameters upon convective heat transfer is studied. The investigation is performed by setting γ at different inclinations while Pr has been assigned a constant value of 6.2. Both nanoparticles and base fluid are in thermal equilibrium and a no slip condition has been assumed between them. Thermophysical properties of nanoparticles Cu and H_2O are kept constant [59].

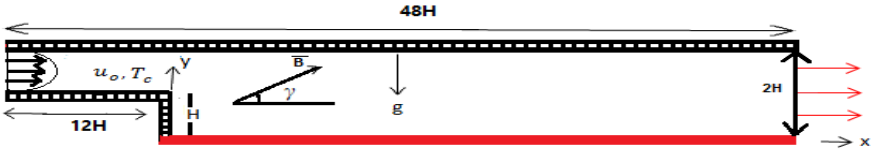

Figure 3.1: Schematic diagram of the physical problem.

Physical Properties	H_2O	Cu
$C_p(J\ kg^{-1}K^{-1})$	4179	383
$k(W\ m^{-1}k^{-1})$	0.6	400
$\beta(k^{-1})$	2.1×10^{-4}	1.67×10^{-5}
$\sigma(\Omega\ m^{-1})$	0.05	5.97×10^{7}
$\rho(kg\ m^{-3})$	997.1	8954

Table 3.1: Thermo physical properties of H_2O and Cu.

3.2 Governing Equations

According to the assumptions above, continuity, momentum and energy equations in dimensional form, are as given below. Also, x and y components of Lorentz force are incorporated in momentum equation.

- **Continuity Equation**

$$\frac{\partial u}{\partial x} + \frac{\partial v}{\partial y} = 0, \tag{3.1}$$

- **x-Component of Momentum Equation**

$$\left(u\frac{\partial u}{\partial x} + v\frac{\partial u}{\partial y}\right) = -\frac{1}{\rho_{nf}}\frac{\partial P}{\partial x} + \nu_{nf}\left(\frac{\partial^2 u}{\partial x^2} + \frac{\partial^2 u}{\partial y^2}\right) + \frac{\sigma_{nf}B_0^2}{\rho_{nf}}(v\sin\gamma\cos\gamma - u\sin^2\gamma), \tag{3.2}$$

- **y-Component of Momentum equation**

$$\left(u\frac{\partial v}{\partial x} + v\frac{\partial v}{\partial y}\right) = -\frac{1}{\rho_{nf}}\frac{\partial P}{\partial y} + \nu_{nf}\left(\frac{\partial^2 v}{\partial x^2} + \frac{\partial^2 v}{\partial y^2}\right) + (\beta)_{nf}\, g\,(T - T_c) + \frac{\sigma_{nf}B_0^2}{\rho_{nf}}(u\sin\gamma\cos\gamma - v\cos^2\gamma), \tag{3.3}$$

- **Energy Equation**

$$u\frac{\partial T}{\partial x} + v\frac{\partial T}{\partial y} = \alpha_{nf}\left(\frac{\partial^2 T}{\partial x^2} + \frac{\partial^2 T}{\partial y^2}\right), \tag{3.4}$$

where, α_{nf} is thermal diffusivity of nanofluids. Viscous dissipation, induced magnetic fields and Joule heating are neglected.

Dimensional Boundary Conditions

The associated boundary conditions are

1. The bottom wall of the step downstream:
   $u = 0, \qquad v = 0, \qquad T = T_h$
2. At the inlet of channel:
   $u = u_0, \qquad v = 0, \qquad T = T_c$
3. At the channel outlet:
   $\frac{\partial u}{\partial x} = 0, \qquad v = 0, \qquad \frac{\partial T}{\partial x} = 0$
4. On the other walls of channels:
   $u = 0, \qquad v = 0, \qquad \frac{\partial T}{\partial n} = 0,$

where, n denotes the direction of the normal.

Nanofluid Properties and used Co-Relation

The other effective properties which may effect and enhance the thermal conductivity of nanofluids are [1] as follow:

- **Effective Density**

$$\rho_{nf} = (1-\phi)\,\rho_f + \phi\rho_p \tag{3.5}$$

- **Specific Heat**

$$(\rho c_\rho)_{nf} = (1-\phi)(\rho c_\rho)_f + \phi(\rho c_\rho)_p \tag{3.6}$$

- **Thermal Expansion Coefficient**

$$(\rho\beta)_{nf} = (1-\phi)(\rho\beta)_f + \phi(\rho\beta)_p \tag{3.7}$$

- **Electrical Conductivity**

$$\sigma_{nf} = (1-\phi)\sigma_f + \phi\sigma_p. \tag{3.8}$$

Subscripts nf, f, and p stands for nanofluid, base fluid and solid particle respectively.

3.3 Dimensionless Form of Governing Equations for Steady Flow with Boundary Conditions

Following are the physical relations used to transform governing equations to the dimensionless form [1, 60]:

$$X = \frac{x}{L}, \quad Y = \frac{y}{L}, \quad U = \frac{u}{u_0}, \quad V = \frac{v}{u_0}, \quad \theta = \frac{T-T_c}{T_h-T_c}, \quad P = \frac{p}{\rho_{nf}{u_0}^2},$$

$$Re = \frac{u_0 L}{\nu_f}, \quad Pr = \frac{\nu_f}{\alpha_f}, \quad Ha = B_0 L\sqrt{\frac{\sigma_f}{\nu_f}}, \quad Ri = \frac{Gr}{Re^2}, \quad Gr = \frac{g\beta\Delta T L^3}{\nu_f^2}.$$

After conversion, the Eqs. (3.1) - (3.4) are transformed to the following dimensionless form:

- **Continuity Equation**

$$\frac{\partial U}{\partial X}+\frac{\partial V}{\partial Y}=0, \tag{3.9}$$

- **x-Component of Momentum Equation**

$$\begin{aligned}\left(U\frac{\partial U}{\partial X}+V\frac{\partial U}{\partial Y}\right)=&-\frac{\partial P}{\partial X}+\frac{\nu_{nf}}{\nu_f}\frac{1}{Re}\left(\frac{\partial^2 U}{\partial X^2}+\frac{\partial^2 U}{\partial Y^2}\right)\\&+\frac{\rho_f}{\rho_{nf}}\frac{\sigma_{nf}}{\sigma_f}\frac{Ha^2}{Re}(V\sin\gamma\cos\gamma-U\sin^2\gamma),\end{aligned} \tag{3.10}$$

- **y-Component of Momentum equation**

$$\begin{aligned}\left(U\frac{\partial V}{\partial X}+V\frac{\partial V}{\partial Y}\right)=&-\frac{\partial P}{\partial Y}+\frac{\nu_{nf}}{\nu_f}\frac{1}{Re}\left(\frac{\partial^2 V}{\partial X^2}+\frac{\partial^2 V}{\partial Y^2}\right)\\&+\frac{\rho_f}{\rho_{nf}}\frac{\sigma_{nf}}{\sigma_f}\frac{Ha^2}{Re}(U\sin\gamma\cos\gamma-V\cos^2\gamma)\\&+\frac{\rho_f}{\rho_{nf}}\frac{(\rho\beta)_{nf}}{(\rho\beta)_f}Ri\theta,\end{aligned} \tag{3.11}$$

- **Energy Equation**

$$U\frac{\partial\theta}{\partial X}+V\frac{\partial\theta}{\partial Y}=\frac{1}{RePr}\frac{\kappa_{nf}}{\kappa_f}\frac{(\rho c_p)_f}{(\rho c_p)_{nf}}\left(\frac{\partial^2\theta}{\partial X^2}+\frac{\partial^2\theta}{\partial Y^2}\right). \tag{3.12}$$

Non-Dimensional Boundary Conditions

1. At the bottom wall of step:

   $U=0, \qquad V=0, \qquad \theta=1.$

2. At the inlet of channel:

   $U=1, \qquad V=0, \qquad \theta=0.$

3. At the channel outlet:

   $\frac{\partial U}{\partial X}=0, \qquad V=0, \qquad \frac{\partial\theta}{\partial X}=0.$

4. On the other walls of channels:

   $U=0, \qquad V=0, \qquad \frac{\partial\theta}{\partial n}=0,$

where, n denotes the direction of the normal.

3.4 Physical Parameters of Interest

Local Nu is calculated at the hot bottom wall through:

$$Nu_l = -\frac{k_{nf}}{k_f}\left(\frac{\partial\theta}{\partial y}\right)_l. \tag{3.13}$$

Averaged Nu is obtained by integrating the local Nu over the heated bottom wall along the downstream direction. It is the mean of all local Nu_l.

$$Nu_{avg} = \frac{1}{L}\int_0^L Nu_l ds. \tag{3.14}$$

Here L is the total length of the heated wall.

3.5 Solution Methodology

FEM is utilized to numerically solve the non linear partial coupled PDEs with corresponding boundary conditions. The geometric domain is divided into non overlapping finite elements. For weak formulation, the dimensional form is converted into dimensionless form through proper transformations. The strong form of the equations is converted into the weak form by multiply PDEs by test functions of the same space and the equations are integrated over the entire domain. The discrete solution is achieved by introducing the finite dimensional test space and trial solution through Galerkin discretization scheme. The finite element pair Q_2/P_1^{disc} satisfies the (LBB) condition of stability. Biquadratic Q_2-element is utilized for temperature and velocity components whereas, P_1^{disc}-element is applied to approximate pressure. Approximations are plugged into the governing laws to obtain residuals for the conservation equations. Also, the non linear momentum terms are simplified by Fixed point iteration method.

3.5.1 Weak/Variational Formulation

Weak formulation or variational formulation is a method by which strong form of dimensional PDEs or physical laws of the problem are converted into integral from. This is done by multiplying a test function or weights with the given PDEs and integrate it over the entire physical domain. We start from the strong form, which is given by:

$$\left(U\frac{\partial U}{\partial X}+V\frac{\partial U}{\partial Y}\right) = -\frac{\partial P}{\partial X}+\frac{\nu_{nf}}{\nu_f Re}\left(\frac{\partial^2 U}{\partial X^2}+\frac{\partial^2 U}{\partial Y^2}\right) + \frac{\rho_f}{\rho_{nf}}\frac{\sigma_{nf}}{\sigma_f}\frac{Ha^2}{Re}(V\sin\gamma\cos\gamma - U\sin^2\gamma), \tag{3.15}$$

$$\left(U\frac{\partial V}{\partial X}+V\frac{\partial V}{\partial Y}\right) = -\frac{\partial P}{\partial Y}+\frac{\nu_{nf}}{\nu_f Re}\left(\frac{\partial^2 V}{\partial X^2}+\frac{\partial^2 V}{\partial Y^2}\right)+\frac{\rho_f}{\rho_{nf}}\frac{(\rho\beta)_{nf}}{(\rho\beta)_f}Ri\theta + \frac{\rho_f}{\rho_{nf}}\frac{\sigma_{nf}}{\sigma_f}\frac{Ha^2}{Re}(U\sin\gamma\cos\gamma - V\cos^2\gamma), \tag{3.16}$$

$$\frac{\partial U}{\partial X}+\frac{\partial V}{\partial Y} = 0, \tag{3.17}$$

$$U\frac{\partial \theta}{\partial X}+V\frac{\partial \theta}{\partial Y} = \frac{1}{RePr}\frac{\kappa_{nf}}{\kappa_f}\frac{(\rho c_p)_f}{(\rho c_p)_{nf}}\left(\frac{\partial^2\theta}{\partial X^2}+\frac{\partial^2\theta}{\partial Y^2}\right). \tag{3.18}$$

Considering the Eqs. (3.15) - (3.18) for week formulation. Multiplying momentum and energy equations by test function $\omega \in \mathbf{W}$ and continuity equation by $q \in Q$ and integrating over whole computational geometry (Ω). $\mathbf{W}$ and Q are test spaces. $\mathbf{W} = [H_1(\Omega)]^3$ is the test space for the components of velocity U, V and temperature θ whereas, $Q = L_2(\Omega)$ is the test space for component of pressure. Thus week formulation is as follows:

Find $(U,V,\theta) \in \mathbf{W}$ and $P \in Q$ such that:

$$-\frac{\nu_{nf}}{\nu_f Re}\int_\Omega\left(\frac{\partial^2 U}{\partial X^2}+\frac{\partial^2 U}{\partial Y^2}\right)\omega d\Omega-\frac{\rho_f}{\rho_{nf}}\frac{\sigma_{nf}}{\sigma_f}\frac{Ha^2}{Re}\int_\Omega(V\sin\gamma\cos\gamma-U\sin^2\gamma)\omega d\Omega$$
$$+\int_\Omega\left(U\frac{\partial U}{\partial X}+V\frac{\partial U}{\partial Y}\right)\omega d\Omega+\int_\Omega\frac{\partial P}{\partial X}\omega d\Omega=0 \tag{3.19}$$

$$-\frac{\nu_{nf}}{\nu_f Re}\int_\Omega\left(\frac{\partial^2 V}{\partial X^2}+\frac{\partial^2 V}{\partial Y^2}\right)\omega d\Omega-\frac{\rho_f}{\rho_{nf}}\frac{\sigma_{nf}}{\sigma_f}\frac{Ha^2}{Re}\int_\Omega(U\sin\gamma\cos\gamma-V\cos^2\gamma)\omega d\Omega$$
$$+\int_\Omega\left(U\frac{\partial V}{\partial X}+V\frac{\partial V}{\partial Y}\right)\omega d\Omega+\int_\Omega\frac{\partial P}{\partial Y}\omega d\Omega-\frac{\rho_f}{\rho_{nf}}\frac{(\rho\beta)_{nf}}{(\rho\beta)_f}Ri\int_\Omega\theta\omega d\Omega=0 \tag{3.20}$$

$$\int_\Omega\left(\frac{\partial U}{\partial X}+\frac{\partial V}{\partial Y}\right)q d\Omega=0, \tag{3.21}$$

$$\int_\Omega\left(U\frac{\partial\theta}{\partial X}+V\frac{\partial\theta}{\partial Y}\right)\omega d\Omega-\frac{1}{RePr}\frac{\kappa_{nf}}{\kappa_f}\frac{(\rho c_p)_f}{(\rho c_p)_{nf}}\int_\Omega\left(\frac{\partial^2\theta}{\partial X^2}+\frac{\partial^2\theta}{\partial Y^2}\right)\omega d\Omega=0, \tag{3.22}$$

for all $(w,q) \in \mathbf{W} \times Q$.

Now, by using Galerkin discretization method, the infinite dimensional test and solution spaces are approximated, i.e.,

$(U_h, V_h, \theta_h, P_h) \approx (U, V, \theta, P)$ whereas, $\mathbf{W} \approx \mathbf{W}_h$ and $Q \approx Q_h$.

The non linear equations are,

$$\frac{\nu_{nf}}{\nu_f Re}\int_\Omega\left(\frac{\partial U_h}{\partial X}\frac{\partial \omega_h}{\partial X}+\frac{\partial U_h}{\partial Y}\frac{\partial \omega_h}{\partial Y}\right)d\Omega+\int_\Omega\left(U_h\frac{\partial U_h}{\partial X}+V_h\frac{\partial U_h}{\partial Y}\right)\omega_h d\Omega$$
$$-\frac{\rho_f}{\rho_{nf}}\frac{\sigma_{nf}}{\sigma_f}\frac{Ha^2}{Re}\int_\Omega(V_h\sin\gamma\cos\gamma-U_h\sin^2\gamma)\omega_h d\Omega-\int_\Omega\frac{\partial \omega_h}{\partial X}P_h d\Omega=0, \tag{3.23}$$

$$\frac{\nu_{nf}}{\nu_f Re}\int_\Omega\left(\frac{\partial V_h}{\partial X}\frac{\partial \omega_h}{\partial X}+\frac{\partial V_h}{\partial Y}\frac{\partial \omega_h}{\partial Y}\right)d\Omega+\int_\Omega\left(U_h\frac{\partial V_h}{\partial X}+V_h\frac{\partial V_h}{\partial Y}\right)\omega_h d\Omega-$$
$$-\frac{\rho_f}{\rho_{nf}}\frac{\sigma_{nf}}{\sigma_f}\frac{Ha^2}{Re}\int_\Omega(U_h\sin\gamma\cos\gamma-V_h\cos^2\gamma)\omega_h d\Omega\int_\Omega\frac{\partial \omega_h}{\partial Y}P_h d\Omega$$
$$-\frac{\rho_f}{\rho_{nf}}\frac{(\rho\beta)_{nf}}{(\rho\beta)_f}Ri\int_\Omega\theta_h\omega_h d\Omega=0, \tag{3.24}$$

$$\int_\Omega\left(\frac{\partial U_h}{\partial X}+\frac{\partial V_h}{\partial Y}\right)\omega_h d\Omega=0, \tag{3.25}$$

$$\int_\Omega\left(U_h\frac{\partial \theta_h}{\partial X}+V_h\frac{\partial \theta_h}{\partial Y}\right)\omega_h d\Omega$$
$$+\frac{1}{RePr}\frac{\kappa_{nf}}{\kappa_f}\frac{(\rho c_p)_f}{(\rho c_p)_{nf}}\int_\Omega\left(\frac{\partial \theta_h}{\partial X}\frac{\partial \omega_h}{\partial X}+\frac{\partial \theta_h}{\partial Y}\frac{\partial \omega_h}{\partial Y}\right)d\Omega=0, \tag{3.26}$$

where,

$$U_h=\sum_{j=1}^{m}U_jS_j,\qquad V_h=\sum_{j=1}^{m}V_jS_j,\qquad \theta_h=\sum_{j=1}^{m}\theta_jS_j,$$
$$P_h=\sum_{k=1}^{n}p_k\eta_k,$$

are the FEM approximated trial functions and

$$w_h=\sum_{i=1}^{m}\omega_iS_i,\qquad q_h=\sum_{l=1}^{n}q_lS_l, \tag{3.27}$$

are the approximated test functions.

Now, for the above four equations, substituting FEM approximations of test and trial functions of U_h, V_h, P_h and θ_h, the fully discretized block matrix is,

$$\begin{bmatrix} A_{11} & b_{12}M & B_1 & 0 \\ b_{21}M & A_{22} & B_2 & b_{24}M \\ {B_1}^T & {B_2}^T & 0 & 0 \\ 0 & 0 & 0 & A_{44} \end{bmatrix} \begin{bmatrix} \underline{U} \\ \underline{V} \\ \underline{P} \\ \underline{\theta} \end{bmatrix} = \begin{bmatrix} \underline{0} \\ \underline{0} \\ \underline{0} \\ \underline{0} \end{bmatrix}, \tag{3.28}$$

where,

$$\begin{aligned} A_{11} &= a_{11}L + b_{11}M - C(U,V), \\ A_{22} &= a_{22}L - b_{22}M - C(U,V), \\ A_{44} &= a_{44}L - C(U,V), \\ a_{11} &= \frac{\nu_{nf}}{\nu_f} = a_{22}, \\ b_{11} &= \frac{\rho_f}{\rho_{nf}}\frac{\sigma_{nf}}{\sigma_f}\frac{Ha^2}{Re}\sin^2\gamma, \\ b_{12} &= -\frac{\rho_f}{\rho_{nf}}\frac{\sigma_{nf}}{\sigma_f}\frac{Ha^2}{Re}\sin\gamma\cos\gamma = b_{21}, \\ b_{22} &= \frac{\rho_f}{\rho_{nf}}\frac{\sigma_{nf}}{\sigma_f}\frac{Ha^2}{Re}\cos^2\gamma, \\ b_{24} &= \frac{\rho_f}{\rho_{nf}}\frac{(\rho\beta)_{nf}}{(\rho\beta)_f}Ri, \\ a_{44} &= \frac{1}{RePr}\frac{\kappa_{nf}}{\kappa_f}\frac{(\rho c_p)_f}{(\rho c_p)_{nf}}. \end{aligned}$$

In the matrix above, L is Laplace matrix, M is the Mass matrix and $C(U,V)$ is the convective matrix. B_1, B_2 are pressure matrices and B_1^T, B_2^T are their transpose. The resulting discrete system of non linear algebraic equations is linearized using the fixed point iteration method and the corresponding linear system is solved by Gaussian elimination method. U and V components of velocity and temperature θ are discretized by Q_2 element having order of accuracy of 3rd degree and P_1^{disc} element having order of accuracy of 2nd degree in L_2 norm respectively. The convergence of the solution is assumed by taking if the relative error for each of the variables fulfill the convergence condition:

$$\left|\frac{\Gamma^{n+1} - \Gamma^n}{\Gamma^{n+1}}\right| \leq 10^{-6} \tag{3.29}$$

Here "n" is for total number of iterations and Γ for any of the dependent variables U, V, P and θ.

3.6 Grid Independence Study

In order to obtain an optimal grid freedom with error-free outcome and minimum computational time, the grid convergence is achieved by selecting several number of elements, is explained by the following table. It tells average Nu computed on bottom wall with highest values of parameters $\gamma = 0°$, $Ri = 0.1$, $\phi = 0.04$, $Pr = 6.5$, $Re = 200$, $Ha = 50$. It is easy to see that solution is transferring successfully from one grid level to the other and solution is converging to the exact solution which seems to be locked at **G5**, as there is less variation in next two levels. The calculated values of average Nusselt number are as shown in **Table** 3.2.

Grid name	No. of elements	Averaged Nusselt number
G1	21	3.105588
G2	84	3.600669
G3	336	3.361771
G4	1344	3.231707
G5	**5376**	**3.208245**
G6	21504	3.205314

Table 3.2: Grid independence study of present work

3.7 Code Validation

The present code is validated in anticipation of the bench mark results checked for reattachment length for recirculation zone X_R over step hight H by keeping Re= 100 and $ER = 2$. **Table** 3.3 presenting $Gr = 0$, $Ri = 0$ and $Gr = 1000$, $Ri = 0.1$ for forced and free convection, respectively over backward facing step with heated bottom wall and adiabatic surrounding. Pr is kept unchanged i.e., 6.5. This table shows that the result are in satisfactory harmony with literary results.

Ri	Present study	Ref. [2]	Ref. [61]	Ref. [62]	Ref. [63]
0.0	4.96875	4.99	4.99	4.97	4.91
0.1	2.96875	3.05	3.05	2.97	3.10

Table 3.3: Reattachment lengths for recirculation region at $Re = 100$.

3.8 Results and Discussion

In this section, numerically imitated outcomes are shown with the help of streamlines, isotherms and Nu, taken against Re, Ha, γ, and ϕ values. The channel is filled out with water as a base fluid and copper nanoparticles. Impact of changing Re for different angles of magnetic field is depicted through streamlines and isotherms, shown by Figures 3.2 and 3.3. Here, $Ha = 25$ and $\phi = 0.02$. When the value of Re increases at $\gamma = 0°$, the flow separates and a recirculation sector appears behind the step, which can be clearly seen in Figure 3.2(a) to 3.2(c). It can be seen that the recirculation sector is occupied in a small region but as the Re rises, the size of the recirculation region expands and velocity of fluid increments. At the low value of Re, the velocity of the fluid is low and viscous forces dominate. On the other hand, increasing Re implies inertial forces are dominated hence, results in augmentation of fluid velocity. As the angle of inclination of magnetic field is increased, the recirculation region seems to be disappearing for $\gamma = 45°$ and $\gamma = 90°$. Now, in case of isotherms, an abruptly changing temperature can be observed near the bottom pallet for the magnetic field angle $\gamma = 0°$ in Figure 3.3(a) to 3.3(c). On increasing angle of inclination of magnetic field more closely packed isotherms near the immediate boundary of the step are observed. This impact gets stonger with growing Reynolds number. For low Reynolds values, a thermal distribution of flow is present in the open area of the channel and this effect gets more dim with higher Re values. It is because growing Re values enhances the flow in the channel it is why sharp thermal difference seems closer to the hot wall of the channel. In contrary, for low Re values, viscous forces are there and thermal boundary layer is visible.

Impact of varying parameters Re, Ha and ϕ is also depicted graphically. Figure 3.4 shows the average heat transfer against different Re within the fluid with regard to γ. Averaged heat transfer has increased with increasing Re and this effect gets stronger with increasing γ values. Increment in averaged heat the transfer is strongly observed for $Re = 200$ as compared to $Re = 20$ for $\gamma = 0°$, $45°$ and $90°$,

respectively. Average Nusselt number is maximum for highest values of Re and γ i.e., at $Re = 200$ and $\gamma = 90°$. Figure 3.5 shows Nu_{avg} against Ha for changing γ values. For $\gamma = 0°$, averaged Nu decreases when Ha increases due to the down fall of the convection. Lorentz forces has caused fluid flow to suppress leading less heat to transfer. Contrary to it, for $\gamma = 90°$, averaged Nu enhances with augmentation of Ha as per flow recirculation behind the step suppresses. The effect is more prominent for high values of Ha. At $\gamma = 45°$, maximum of mean or averaged Nu is obtained, for optimum value of $Ha = 30$. It has been noted that for $\gamma = 45°$ and $90°$, maximum of averaged Nu is obtained at $Ha = 30$ and $Ha = 50$, respectively in comparison with $Ha = 0$. Averaged heat transfer against ϕ is plotted in Figure 3.6 for different values of γ. It has been realized that Nu_{avg} linearly increases with ϕ. For $\phi = 0.04$, increment in Nu_{avg} is maximum for all magnetic field orientations, i.e., $\gamma = 0°$, $45°$ and $90°$ instead of $\phi = 0.0$ and 0.02. It is because, increasing number of nanoparticles will consequently raise the thermal conductivity of the fluid.

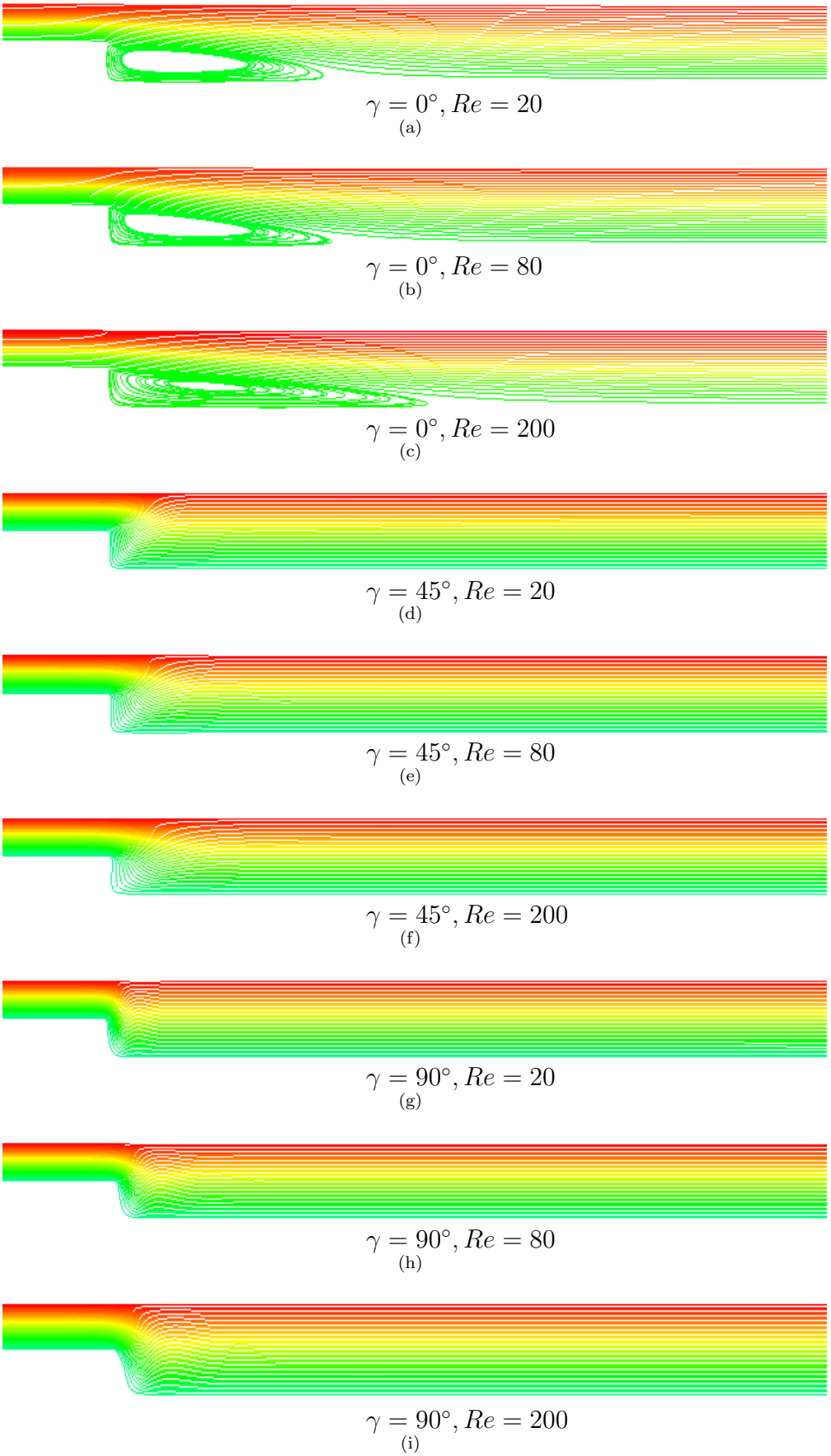

Figure 3.2: Streamlines (a) for different Re at $Ha = 20$, $Ri = 0.1$ and $\phi = 0.02$ for various γ.

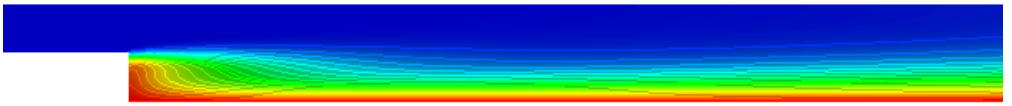

$\gamma = 0°, Re = 20$
(a)

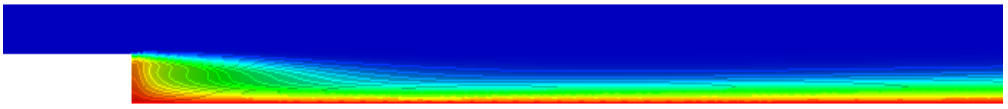

$\gamma = 0°, Re = 80$
(b)

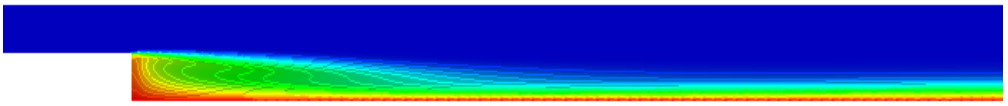

$\gamma = 0°, Re = 200$
(c)

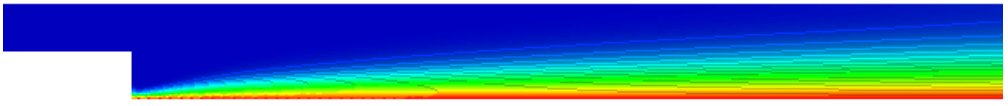

$\gamma = 45°, Re = 20$
(d)

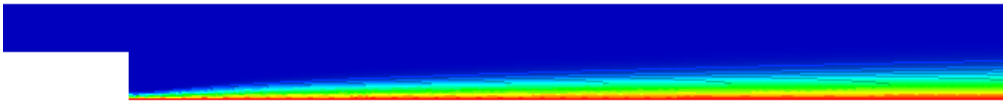

$\gamma = 45°, Re = 80$
(e)

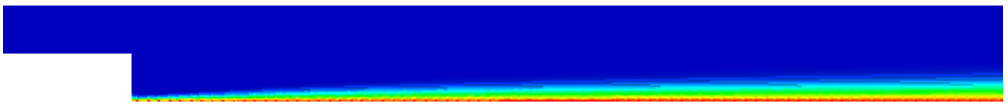

$\gamma = 45°, Re = 200$
(f)

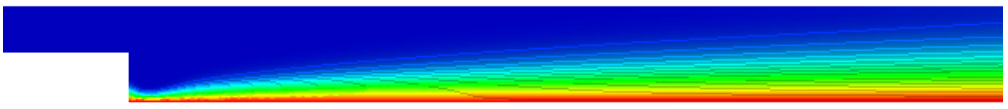

$\gamma = 90°, Re = 20$
(g)

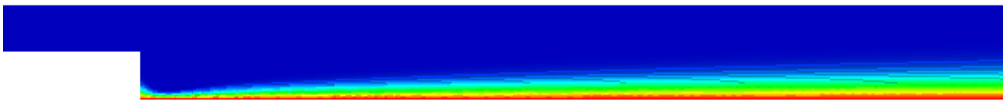

$\gamma = 90°, Re = 80$
(h)

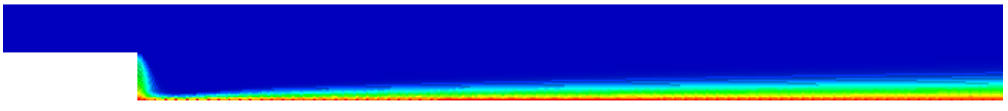

$\gamma = 90°, Re = 200$
(i)

Figure 3.3: Isotherms (b) for different Re at $Ha = 20$, $Ri = 0.1$ and $\phi = 0.02$ for various γ.

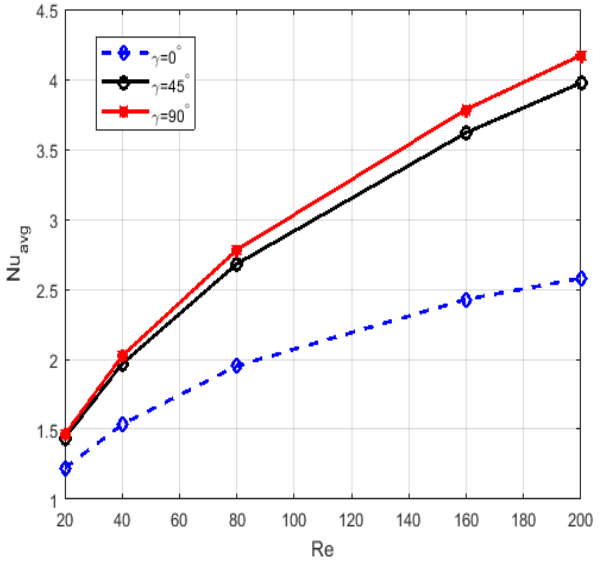

Figure 3.4: Nu_{avg} for different γ as function of Re

.

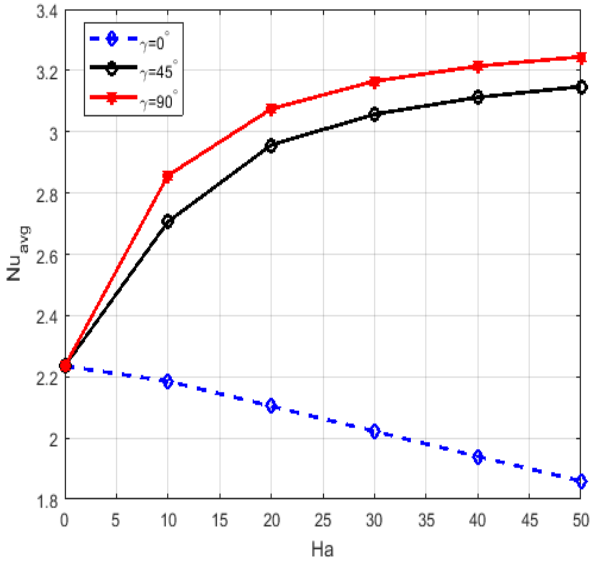

Figure 3.5: Nu_{avg} for different γ as function of Ha

.

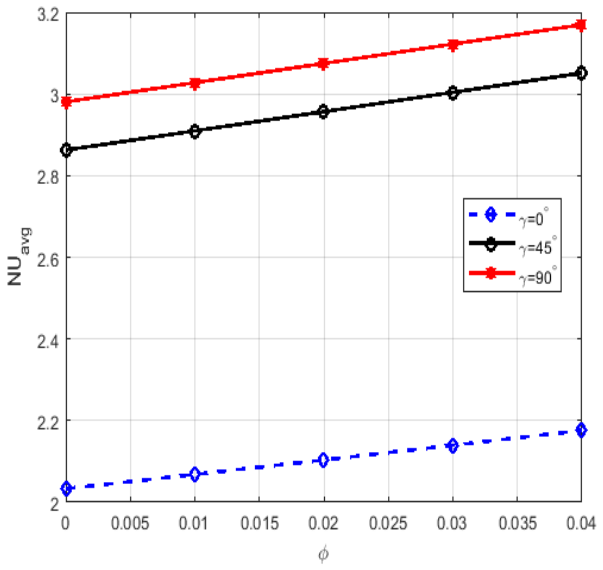

Figure 3.6: Nu_{avg} for different γ as function of ϕ

.

Chapter 4

MHD Mixed Convection Nanofluid Flow with Joule Heating Effect over Porous Backward Facing Step

Porous media is receiving considerable importance in engineering both in chemical and mechanical [64]. Heat transfer in porous medium with combined convection flow in channels and cavities, is one of important application in engineering. Among many other applications fibrous insulation [41], food storage [64] and thermal insulation in buildings [64] are also involved.

The transport principle and flow through porous media have been studied at a wider scale. On performing experiments at industrial and laboratory level these medium are exposed to several processes for example heat transfer, absorption and electrical charges etc. Mathematical modelling of such problems require understanding the behaviour of these media. Because of that scientists and researchers are paying critical attention in this regard.

A lot of research has been carried out on porous media specially with turbulent model over BFS but laminar flow with this configuration has been given less attention. This chapter is based on the study of introducing the porosity in laminar

forced convection flow regime and Joule heating effects in the research priorly conducted by Selimefendigil and Öztop [31].

To solve the governing equations by FEM, weak formulation is required. For this purpose, the non linear dimensional form of equations is transformed into dimensionless form. Strong form of equations is multiplied with the suitable test functions and integrated over whole domain. Approximated solution is achieved through Galerkin discretization method. Thermal behaviour and flow pattern are studied under Joule heating effect and porous medium.

4.1 Physical Model

The present configuration is two dimensional backward facing step having mixed convection MHD nanofluids, with porous medium completely intact inside the entire channel. The physical configuration is reconstructed by considering the fluid to be viscous, incompressible and Newtonian whereas, flow is taken to be laminar and steady state. The hot plate is of the length $10H$ and entire length of the channel is $13H$. Velocity of the flow at the inlet of channel is u_0 and is maintained at a uniform temperature $T = T_c$. Except the bottom wall of step having the temperature $T = T_h$, all the other walls of the channel are adiabatic. The channel contains Cu-water nanofluid, flowing under an oriented magnetic field. The angle of inclination is γ. A schematic diagram is shown in Figure 4.1. Darcy-Brinkman-Forchheimer model has been utilized to model momentum equation for the proposed problem. Particles of porous medium are isotropic solid and Cu-water nanofluid is considered to be homogeneous mixture. Both nanoparticles and base fluid are in thermal equilibrium and a no slip condition has been assumed between them. Effects of thermal radiation, internal heat generation and viscous dissipation are ignored. Boussinesq approximation is applied to overcome the density variations within fluid. Thermophysical properties of nanoparticles Cu and H_2O are kept constant [59].

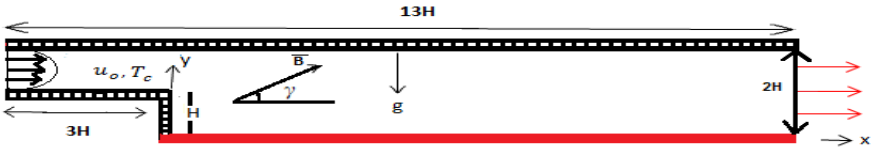

Figure 4.1: Schematic diagram of the physical model.

4.2 Dimensional Governing Equations

When a fluid that is electrically conducting, passes through a magnetic field, a current is induced. This induced current generates an action force on the fluid. As a consequence, a reaction force is produced, called the Lorentz force. The electromagnetic force or Lorentz force possessed by the fluid is $\mathbf{F} = \sigma(\mathbf{U} \times \mathbf{B}) \times \mathbf{B}$ [65], where, σ is electrical conductivity of the fluid, $\mathbf{U}$ is the velocity of fluid and $\overline{B}$ is the uniform magnetic field, comprised of the components $(\mathbf{B}_x, \mathbf{B}_y)$, i.e., $\mathbf{B}_x = B_0 \cos\gamma$ and $\mathbf{B}_y = B_0 \sin\gamma$ [66] along x and y axes, respectively. Here, B_0 is the magnitude of magnetic field. Since, the fluid is electrically conducting because of magmatic field effects. So, the last terms in Eq. (4.2) and Eq. (4.3) symbolize Lorentz force. This force produces dissipated energy in terms of viscous dissipation and Joule heating. In Eq. (4.4), the last term portrays the Joule heating effect, where viscous dissipation is neglected.

Under the preceding assumptions, the governing equations of the physical model are given by:

- **Continuity Equation**

$$\frac{\partial u}{\partial x}+\frac{\partial v}{\partial y}=0, \tag{4.1}$$

- **x-Component of Momentum Equation**

$$\begin{aligned}\frac{1}{\epsilon^2}\left(u\frac{\partial u}{\partial x}+v\frac{\partial u}{\partial y}\right)=&-\frac{1}{\rho_{nf}}\frac{\partial P}{\partial x}+\frac{\nu_{nf}}{\epsilon}\left(\frac{\partial^2 u}{\partial x^2}+\frac{\partial^2 u}{\partial y^2}\right)-\frac{\mu_{nf}}{K\rho_{nf}}u\\&-\frac{1.75}{\sqrt{150K}\epsilon^{\frac{3}{2}}}\left(\sqrt{u^2+v^2}\right)u+\frac{\sigma_{nf}B_0^2}{\rho_{nf}}(v\sin\gamma\cos\gamma-u\sin^2\gamma),\end{aligned} \tag{4.2}$$

- **y-Component of Momentum Equation**

$$\begin{aligned}\frac{1}{\epsilon^2}\left(u\frac{\partial v}{\partial x}+v\frac{\partial v}{\partial y}\right)=&-\frac{1}{\rho_{nf}}\frac{\partial P}{\partial y}+\frac{\nu_{nf}}{\epsilon}\left(\frac{\partial^2 v}{\partial x^2}+\frac{\partial^2 v}{\partial y^2}\right)-\frac{\mu_{nf}}{K\rho_{nf}}v\\&+(\beta)_{nf}\,g\,(T-T_c)-\frac{1.75}{\sqrt{150K}\epsilon^{\frac{3}{2}}}\left(\sqrt{u^2+v^2}\right)v\\&+\frac{\sigma_{nf}B_0^2}{\rho_{nf}}(u\sin\gamma\cos\gamma-v\cos^2\gamma),\end{aligned} \tag{4.3}$$

- **Energy Equation**

$$u\frac{\partial T}{\partial x}+v\frac{\partial T}{\partial y}=\alpha_{nf}\left(\frac{\partial^2 T}{\partial x^2}+\frac{\partial^2 T}{\partial y^2}\right)+\frac{\sigma_{nf}B_0^2}{(\rho c_p)_{nf}}(u\sin\gamma-v\cos\gamma)^2. \tag{4.4}$$

Dimensional Boundary Conditions

The dimensional form of the boundary conditions of the problem are:

1. On the bottom wall of the step downstream:

   $u=0, \qquad v=0, \qquad T=T_h$

2. At the inlet of channel:

   $u=u_0, \qquad v=0, \qquad T=T_c$

3. At the channel outlet:

   $\frac{\partial u}{\partial x}=0, \qquad v=0, \qquad \frac{\partial T}{\partial x}=0$

4. On the other walls of channels:

$$u = 0, \qquad v = 0, \qquad \frac{\partial T}{\partial n} = 0$$

where, n denotes the direction of the normal.

4.3 Dimensionless Governing Equations with Boundary Conditions

Following are the transformation parameters for the physical laws to convert them into the dimensionless form [1, 60, 67]:

$$X = \frac{x}{L}, \quad Y = \frac{y}{L}, \quad U = \frac{u}{u_0}, \quad V = \frac{v}{u_0}, \quad \theta = \frac{T - T_c}{T_h - T_c}, \quad P = \frac{p}{\rho_{nf} {u_0}^2},$$

$$Re = \frac{u_0 L}{\nu_f}, \quad Da = \frac{K}{L^2}, \quad Pr = \frac{\nu_f}{\alpha_f}, \quad Ri = \frac{Gr}{Re^2}, \quad Gr = \frac{g\beta\Delta T L^3}{\nu_f^2},$$

$$Ec = \frac{u_0^2}{(c_p)_f (T_h - T_c)}, \quad Ha = B_0 L \sqrt{\frac{\sigma_f}{\nu_f}}.$$

After conversion, the Eqs. (4.1) - (4.4) are transformed to the following dimensionless form:

- **Continuity Equation**

$$\frac{\partial U}{\partial X} + \frac{\partial V}{\partial Y} = 0, \tag{4.5}$$

- **x-Component of Momentum Equation**

$$\begin{aligned} \frac{1}{\epsilon^2}\left(U\frac{\partial U}{\partial X} + V\frac{\partial U}{\partial Y}\right) = &- \frac{\partial P}{\partial X} + \frac{\nu_{nf}}{\nu_f}\frac{1}{\epsilon Re}\left(\frac{\partial^2 U}{\partial X^2} + \frac{\partial^2 U}{\partial Y^2}\right) \\ &- \frac{\mu_{nf}}{\rho_{nf}\nu_f}\frac{1}{ReDa}U - \frac{1.75}{\sqrt{150Da\epsilon^3}}\sqrt{U^2 + V^2}U \\ &+ \frac{\rho_f}{\rho_{nf}}\frac{\sigma_{nf}}{\sigma_f}\frac{Ha^2}{Re}(V\sin\gamma\cos\gamma - U\sin^2\gamma), \end{aligned} \tag{4.6}$$

- **y-Component of Momentum Equation**

$$\begin{aligned}\frac{1}{\epsilon^2}\left(U\frac{\partial V}{\partial X}+V\frac{\partial V}{\partial Y}\right) =& -\frac{\partial P}{\partial Y}+\frac{\nu_{nf}}{\nu_f}\frac{1}{\epsilon Re}\left(\frac{\partial^2 V}{\partial X^2}+\frac{\partial^2 V}{\partial Y^2}\right)\\ &-\frac{\mu_{nf}}{\rho_{nf}\nu_f}\frac{1}{ReDa}V-\frac{1.75}{\sqrt{150Da}\epsilon^{\frac{3}{2}}}\sqrt{U^2+V^2}V\\ &+\frac{\rho_f}{\rho_{nf}}\frac{\sigma_{nf}}{\sigma_f}\frac{Ha^2}{Re}(U\sin\gamma\cos\gamma-V\cos^2\gamma)\\ &+\frac{\rho_f}{\rho_{nf}}\frac{(\rho\beta)_{nf}}{(\rho\beta)_f}Ri\theta, \end{aligned} \tag{4.7}$$

- **Energy Equation**

$$\begin{aligned}U\frac{\partial\theta}{\partial X}+V\frac{\partial\theta}{\partial Y} =& \frac{1}{RePr}\frac{\kappa_{nf}}{\kappa_f}\frac{(\rho c_p)_f}{(\rho c_p)_{nf}}\left(\frac{\partial^2\theta}{\partial X^2}+\frac{\partial^2\theta}{\partial Y^2}\right)\\ &+\frac{\sigma_{nf}}{\sigma_f}\frac{(\rho c_p)_f}{(\rho c_p)_{nf}}\frac{Ha^2}{Re}Ec(U\sin\gamma-V\cos\gamma)^2. \end{aligned} \tag{4.8}$$

Non-Dimensional Boundary Conditions

Following are the corresponding non-dimensional boundary conditions given by:

1. At the bottom wall of step:
   $U=0, \qquad V=0, \qquad \theta=1$
2. At the inlet of channel:
   $U=1, \qquad V=0, \qquad \theta=0$
3. At the channel outlet:
   $\frac{\partial U}{\partial X}=0, \qquad V=0, \qquad \frac{\partial\theta}{\partial X}=0$
4. On the other walls of channels:
   $U=0, \qquad V=0, \qquad \frac{\partial\theta}{\partial n}=0$

where, n denotes the direction of the normal.

4.4 Physical Parameters of Interest

Local Nu is given as:

$$Nu_l = -\frac{k_{nf}}{k_f}\left(\frac{\partial\theta}{\partial y}\right)_l.$$

Averaged Nu is obtained by integrating the local Nu_l over the entire heated wall:

$$Nu_{avg} = \frac{1}{L}\int_0^L Nu_l ds,$$

where L is the length of hot wall.

4.5 Solution Methodology

Non linear dimensionless form of the governing PDEs (4.5) - (4.8) of the physical problem are solved using finite element method. First, weak formulation of the equations ia achieved by multiplying them with suitable test functions and integrating them over the whole domain. Solution and test spaces are approximated by using Galerkin discretization. These approximations of test and trial functions are substituted into the discretized non linear weak form in order to get fully discretized algebraic equations. The solution steps are explained as follows:

4.5.1 Strong Form

The strong form of governing equations can be rewritten as follows:

$$\Delta_1\left(U\frac{\partial U}{\partial X}+V\frac{\partial U}{\partial Y}\right)=-\frac{\partial P}{\partial X}+a_{11}\left(\frac{\partial^2 U}{\partial X^2}+\frac{\partial^2 U}{\partial Y^2}\right)-\Delta_2 U-\Delta_3 U + \Delta_4(V\sin\gamma\cos\gamma-U\sin^2\gamma), \tag{4.9}$$

$$\Delta_1\left(U\frac{\partial V}{\partial X}+V\frac{\partial V}{\partial Y}\right)=-\frac{\partial P}{\partial Y}+a_{22}\left(\frac{\partial^2 V}{\partial X^2}+\frac{\partial^2 V}{\partial Y^2}\right)-\Delta_2 V-\Delta_3 V + \Delta_4(U\sin\gamma\cos\gamma-V\cos^2\gamma)+b_{24}\theta, \tag{4.10}$$

$$\frac{\partial U}{\partial X}+\frac{\partial V}{\partial Y}=0, \tag{4.11}$$

$$U\frac{\partial \theta}{\partial X}+V\frac{\partial \theta}{\partial Y}=a_{44}\left(\frac{\partial^2 \theta}{\partial X^2}+\frac{\partial^2 \theta}{\partial Y^2}\right)+\Delta_5(U\sin\gamma-V\cos\gamma)^2, \tag{4.12}$$

where,

$$\begin{aligned}
\Delta_1 &= \frac{1}{\epsilon^2},\\
\Delta_2 &= \frac{\mu_{nf}}{\rho_{nf}\nu_f}\frac{1}{ReDa},\\
\Delta_3 &= \frac{1.75}{\sqrt{150Da}\epsilon^{\frac{3}{2}}}\sqrt{U^2+V^2},\\
\Delta_4 &= \frac{\rho_f}{\rho_{nf}}\frac{\sigma_{nf}}{\sigma_f}\frac{Ha^2}{Re},\\
\Delta_5 &= \frac{\sigma_{nf}}{\sigma_f}\frac{(\rho c_p)_f}{(\rho c_p)_{nf}}\frac{Ha^2}{Re}Ec,\\
a_{11} &= \frac{\nu_{nf}}{\nu_f}\frac{1}{Re}=a_{22},\\
a_{44} &= \frac{1}{RePr}\frac{\kappa_{nf}}{\kappa_f}\frac{(\rho c_p)_f}{(\rho c_p)_{nf}},\\
b_{24} &= \frac{\rho_f}{\rho_{nf}}\frac{(\rho\beta)_{nf}}{(\rho\beta)_f}Ri.
\end{aligned}$$

4.5.2 Weak Form

In order to obtain weak formulation multiplying the momentum and energy equations by test function $\omega \in \mathbf{W}$ and continuity equation by $q \in Q$ and integrating over whole computational domain (Ω). Integration by parts is done by applying Green's Identity. $\mathbf{W}$ and Q are infinite dimensional test spaces where, ω and q are respective test functions of corresponding test spaces. $\mathbf{W} = [H_1(\Omega)]^3$ is the test space for the velocity U, V and for temperature θ and $Q = L_2(\Omega)$ is the test space for the of pressure. Thus weak formulation is as follows:
Find (U,V,θ) $\in \mathbf{W}$ and $P \in Q$ such that:

$$\Delta_1 \int_\Omega \left(U\frac{\partial U}{\partial X} + V\frac{\partial U}{\partial Y} \right) \omega d\Omega + \int_\Omega \frac{\partial P}{\partial X}\omega d\Omega - a_{11}\int_\Omega \left(\frac{\partial^2 U}{\partial X^2} + \frac{\partial^2 U}{\partial Y^2} \right) \omega d\Omega$$
$$+ \Delta_2 \int_\Omega U\omega d\Omega + \Delta_3 \int_\Omega U\omega d\Omega - \Delta_4 \int_\Omega (V\sin\gamma\cos\gamma - U\sin^2\gamma)\omega d\Omega = 0, \quad (4.13)$$

$$\Delta_1 \int_\Omega \left(U\frac{\partial V}{\partial X} + V\frac{\partial V}{\partial Y} \right) \omega d\Omega + \int_\Omega \frac{\partial P}{\partial Y}\omega d\Omega - a_{22}\int_\Omega \left(\frac{\partial^2 V}{\partial X^2} + \frac{\partial^2 V}{\partial Y^2} \right) \omega d\Omega$$
$$+ \Delta_2 \int_\Omega V\omega d\Omega + \Delta_3 \int_\Omega V\omega d\Omega - \Delta_4 \int_\Omega (U\sin\gamma\cos\gamma - V\cos^2\gamma)\omega d\Omega$$
$$- b_{24}\int_\Omega \theta\omega d\Omega = 0, \quad (4.14)$$

$$\int_\Omega \left(\frac{\partial U}{\partial X} + \frac{\partial V}{\partial Y} \right) q d\Omega = 0, \quad (4.15)$$

$$\int_\Omega \left(U\frac{\partial \theta}{\partial X} + V\frac{\partial \theta}{\partial Y} \right) \omega d\Omega + a_{44}\int_\Omega \left(\frac{\partial^2 \theta}{\partial X^2} + \frac{\partial^2 \theta}{\partial Y^2} \right) \omega d\Omega$$
$$+ \Delta_5 \int_\Omega (U\sin\gamma - V\cos\gamma)^2 \omega d\Omega = 0 \quad (4.16)$$

for all $w \in \mathbf{W}$ and $q \in Q$.
being the Galerkin method, test and trial spaces are chosen as same. By using Galerkin discretization, the infinite dimensional test and solution spaces are approximated i.e., $(U_h, V_h, \theta_h, P_h) \approx (U, V, \theta, P)$, whereas, $\mathbf{W} \approx \mathbf{W}_h$ and $Q \approx Q_h$.

At discrete level, the weak form of the equations is as under:

Find $(U_h,V_h,\theta_h) \in \mathbf{W}$ and $P_h \in Q$ such that:

$$a_{11}\int_\Omega \left(\frac{\partial U_h}{\partial X}\frac{\partial \omega_h}{\partial X}+\frac{\partial U_h}{\partial Y}\frac{\partial \omega_h}{\partial Y}\right)d\Omega - \int_\Omega \frac{\partial \omega_h}{\partial X}P_h d\Omega$$
$$+\Delta_1\int_\Omega \left(U_h\frac{\partial U_h}{\partial X}+V_h\frac{\partial U_h}{\partial Y}\right)\omega_h d\Omega + \Delta_2\int_\Omega U_h\omega_h d\Omega + \Delta_3\int_\Omega U_h\omega_h d\Omega$$
$$-\Delta_4\int_\Omega (V_h\sin\gamma\cos\gamma - U_h\sin^2\gamma)\omega_h d\Omega = 0, \tag{4.17}$$

$$a_{22}\int_\Omega \left(\frac{\partial V_h}{\partial X}\frac{\partial \omega_h}{\partial X}+\frac{\partial V_h}{\partial Y}\frac{\partial \omega_h}{\partial Y}\right)d\Omega - \int_\Omega \frac{\partial \omega_h}{\partial Y}P_h d\Omega$$
$$+\Delta_1\int_\Omega \left(U_h\frac{\partial V_h}{\partial X}+V_h\frac{\partial V_h}{\partial Y}\right)\omega_h d\Omega + \Delta_2\int_\Omega V_h\omega_h d\Omega + \Delta_3\int_\Omega V_h\omega_h d\Omega$$
$$-\Delta_4\int_\Omega (U_h\sin\gamma\cos\gamma - V_h\cos^2\gamma)\omega_h d\Omega - b_{24}\int_\Omega \theta_h\omega_h d\Omega = 0, \tag{4.18}$$

$$\int_\Omega \left(\frac{\partial U_h}{\partial X}+\frac{\partial V_h}{\partial Y}\right)q_h d\Omega = 0, \tag{4.19}$$

$$\int_\Omega \left(U_h\frac{\partial \theta_h}{\partial X}+V_h\frac{\partial \theta_h}{\partial Y}\right)\omega_h d\Omega + a_{44}\int_\Omega \left(\frac{\partial \theta_h}{\partial X}\frac{\partial \omega_h}{\partial X}+\frac{\partial \theta_h}{\partial Y}\frac{\partial \omega_h}{\partial Y}\right)d\Omega$$
$$+\Delta_5\int_\Omega (U_h\sin\gamma - V_h\cos\gamma)^2\omega d\Omega \tag{4.20}$$

for all $w_h \in \mathbf{W}_h$ and $q_h \in Q_h$.

Now the FEM approximated trial functions are

$$U_h = \sum_{j=1}^{m} U_j S_j, \qquad V_h = \sum_{j=1}^{m} V_j S_j, \qquad \theta_h = \sum_{j=1}^{m} \theta_j S_j,$$
$$P_h = \sum_{k=1}^{n} p_k \eta_k,$$

and the FEM approximated test functions are

$$w_h = \sum_{i=1}^{m} \omega_i S_i, \qquad q_h = \sum_{l=1}^{n} q_l \eta_l.$$

Next, substituting the FEM approximations of test and trial functions of U_h, V_h, P_h and θ_h into Eqs. (4.17) - (4.20), the fully discretized system of non linear

algebraic equations given by the following block matrix:

$$\begin{bmatrix} A_{11} & b_{12}M & B_1 & 0 \\ b_{21}M & A_{22} & B_2 & b_{24} \\ {B_1}^T & {B_2}^T & 0 & 0 \\ b_{41} & b_{42} & 0 & A_{44} \end{bmatrix} \begin{bmatrix} \underline{U} \\ \underline{V} \\ \underline{P} \\ \underline{\theta} \end{bmatrix} = \begin{bmatrix} \underline{0} \\ \underline{0} \\ \underline{0} \\ \underline{0} \end{bmatrix}, \tag{4.21}$$

$$\begin{aligned} A_{11} &= a_{11}L + \Delta_1 C(U,V) + b_{11}M \\ A_{22} &= a_{22}L + \Delta_1 C(U,V) + b_{22}M \\ A_{44} &= a_{44}L + C(U,V) \\ b_{11} &= \Delta_2 + \Delta_3 - \Delta_4 \sin^2\gamma \\ b_{22} &= \Delta_2 + \Delta_3 - \Delta_4 \cos^2\gamma \\ b_{12} &= -\Delta_4 \sin\gamma\cos\gamma = b_{21} \end{aligned} \tag{4.22}$$

Here, in the block matrix, L, M and $C(U,V)$ represent Laplace, mass and convective matrices respectively. B_1 and B_2 are the pressure matrices and B_1^T , B_2^T are their respective transpose. Alos, b_{41} and b_{42} are corresponding co-efficients of the block matrix. The discrete system thus obtained of non linear algebraic equations is linearized by the fixed point iterations and the Gussian elimination method ia applied to solve the linear system. Velocity components and temperature are discretized with the biquadratic Q_2-element and pressure is discretized using discontinuous linear P_1^{disc}-element. The biquadratic Q_2-element is of third order accuracy whereas linear P_1^{disc}-element has an accuracy of second order. The convergence of the solution is assumed as discussed in earlier in **Chapter 3**.

$$\left|\frac{\Gamma^{n+1} - \Gamma^n}{\Gamma^{n+1}}\right| \leq 10^{-6}. \tag{4.23}$$

"n" represents total number of iterations and Γ represents the dependent variables U, V, P and θ.

4.6 Results and Discussion

Impact of Joule heating on mixed convection in a porous channel has been interpreted numerically in this chapter. The channel is filled with Cu-water nanofluids. Governing parameters are assigned the values ranging, $(0 \leq Ha \leq 100)$, $(0.2 \leq \epsilon \leq 1)$, $(10^{-4} \leq Da \leq 10^{-1})$, $(10^{-6} \leq Ec \leq 10^{-2})$, $(0.00 \leq \phi \leq 0.04)$ and $(0^{\circ} \leq \gamma \leq 90^{\circ})$, other than these are mentioned. Fixed value of 6.2 has been assigned to Pr. Influence of these active parameters has also been conferred through streamlines, isotherms and Matlab graphs for Nu_{avg}.

Impact of altering Ha for inclinations $\gamma = 0^{\circ}$ to 90° is characterized by the Figures 4.2 and 4.3, depicting streamlines and isotherms, respectively. Rest of the quantities were secured to be fixed, $\phi = 0.04$, $\gamma = 0^{\circ}$, $\epsilon = 1$ and $Ri = 1$. The Hartmann number Ha represents the magnetic field strength, put on externally. Initially, in the absence of magnetic field, only natural and forced convection are contributing. Because of which buoyancy and shear forces, both are influencing the flow. Fluid's flow descends down, following the path along the downstream near the hot plate. In addition, flow recirculation occurs behind the step. As the Ha value rises from 25 to 100, the Lorentz force comes into action, as a result the flow is suppressed and streamlines have become flattened, toped up over one another. The phenomena is more pronounced with growing Ha and recirculation behind the step expands. Motion of the fluid under weak shear forces has become weaken due to this force and results in the reduction of fluid velocity. Hence, the reduction in heat transfer is obtained with augmentation in Ha. Isotherms sketches are demonstrated in Figure 4.3. Thermal boundary layer is strictly confined to the hot plate, can be visualised clearly. The flow is almost similar for all Ha values as isotherm contours are approximately the same. At the reattachment point, sharp thermal differences can be seen. Besides, isotherms are assembled near the hot wall with increasing Ha values. This indicates a decrease in heat transfer.

Influence of Ec on streamlines and isotherms are displayed in Figures 4.4 and 4.5, respectively. Since, heat is produced due to viscous dissipation. This causes temperature to rise and ultimately increases fluid velocity. Flow circulation arises in rear of the step and temperature near hot plate raises. Further, streamlines have gone parallel. Positive Ec indicates heating of the fluid i.e., heat from the heating walls into the fluid. Raising Ec, thermal energy is utilized to increase the kinetic energy of the nanoparticles, leaving less heat to transfer. Accordingly, thermal energy dissipates causing thermal heating losses and make it possible to reduce heat transfer. It is because of that reason the temperature field in Figure 4.5, a steep temperature gradient is observable near the hot bottom wall of the channel and a less variation is witnessed for the upper adiabatic plate.

Porosity parameter impacts are illustrated in Figures 4.6 and 4.7, respectively. A noteworthy change is observed in both thermal and flow patterns when the ϵ runs from 0.2 to 0.8. As porosity and permeability are linearly related, therefore they are proportional to each other. At first, at $\epsilon = 0.2$, the recirculation sector is noticeable. This sector, located before reattachment point, decreases for the values from 0.4 to 0.6 and is replaced by the coarse distribution of stream patterns near the step. This indicates that the flow penetrates more quickly in the porous walls of the channel. At $\epsilon = 0.8$ at the inlet of the channel and near the step, streamlines are more crowded, specifying convincing inlet velocity and the flow. For isotherms in Figure 4.7, the flow stratifies thermally and coarser clustering of temperature distribution is seen near the lower hot wall, depicting that the elevated temperature zone is near the heating plate. This fact has become more compact and narrow at the reattachment point in the downstream direction of the flow, for the larger porosity parameter value.

Effect of Da for streamlines and isotherms is unfolded in Figures 4.8 and 4.9, respectively. For $Da = 10^{-4}$, a recirculation area is observable behind the step. It may be noticed that recirculation region is small for this low Da value. This behaviour continues to augment with increasing values of Da. As this value reaches

to its highest value $Da = 10^{-1}$, fluid recirculation reaches to its maximum value. Obviously, high Da, implies high permeability, allowing fluid to move more quickly through pores of porous material and less resistance is offered to the flowing fluid through porous medium. Consequently, results in enhancement in the velocity of the fluid. The thermal pattern for varying Da is observable in Figure 4.9. Thermal distribution seems to confined in the nigh of the step and the bottom wall of the channel by the lengthways direction. Thermal boundary layer is thin for almost all Da values.

The Figures 4.10 to 4.14 present graphically the repercussions of these parameters upon average heat transfer.

Impact of Ha upon average heat transfer of the fluid has been displayed in Figure 4.10. It has been observed that in the beginning, average Nusselt declines gently with exalting Ha at $\gamma = 0°$. A different trend has been found for $\gamma = 45°$ and $90°$. In both the cases, Nu_{avg} rises and is emphasised. This implication is more intense for $\gamma = 90°$ as compared to $\gamma = 45°$. At $\gamma = 0°$, initially Ha is less strong allowing Nu_{avg} to decline gradually. Latterly, due to strong magnetic field, in the view of Lorentz forces the flow dampens and there is less heat to flow. Further, Richardson number is taken to be fixed at unity, therefore combined convection is there. At $\gamma = 0°$, applied magnetic field offers retardation to the transfer of heat and the flow. Buoyancy forces are ceased and shear forces have dominated. That tells heat transfer takes place through conduction. Consequently, averaged Nusselt has been declined. But as soon as γ is elevated, i.e., for $45°$ and $90°$, convection gets excited. The fact is that at high γ value, flow of the fluid gets strong inside the channel. Due to this thermal differences within the fluid enhances and temperature distributes inside the channel. As a result Nu_{avg} is enhanced.

Figure 4.11 determines the influence of Ha upon Na_{avg} for varying ϕ. It reflects that the heat transfer declines for all values of ϕ, as long as Ha is increased. This is because Ha has the tendency of reducing buoyant forces in cavities and channels. Since, heat transfer augments with exalting nanoparticles volume concentration because of their thermal conductivity which decays when exposed to magnetic

field. For lower values of $Ha = 0$ to 25, this effect seems to be less and gets stronger for higher values of $Ha = 25$ to 100. Delineating that with every pour of nanoparticles volume fraction at $Ha = 25$, heat transport of the particles lessens by the virtue of Lorentz force. This fact is similar for whole volume fractions of nanoparticles.

In Figure 4.12, a standard behaviour of Nu_{avg} against Ec is observable. The Nu_{avg} decreases linearly with increasing values of Ec. With every increased ϕ, an augmentation in Nu_{avg} is observed which drops linearly with exalting Ec. It is because of frictional forces present between the nanoparticles, thermal energy has dissipated that leaves less heat to transfer. Average Nusselt is apex for $\phi = 0.04$ as compared to $\phi = 0$ and 0.02.

Nu_{avg} has been shown in Figure 4.13 under the implication of ϵ with diversifying ϕ values. It is obvious that by rising porosity means rising permeability that allows more fluid to flow. This leads to the fact that for more fluid penetration and more thermal conductivity is submitted in the fluid. Indeed offers high convection. In the same way, as the ϵ keeps on exalting from 0.2 to 1.0, averaged Nu keeps on raising. This behaviour is likely, as well as pronounced for entire levels of volume concentration ϕ. Supreme value for Nu_{avg} is found to be at $\epsilon = 1.0$ for $\phi = 0.04$.

Figure 4.14 explains consequences of Da upon heat transfer. Average Nusselt number has declined with exalting Darcy number. In the beginning, declination of Nu_{avg} is faster for every volume fraction. The trend become less intense and linear afterwards for increasing Da. The behaviour is similar for all cases of ϕ for $Da = 10^{-2}$. At the start, low permeability provides more hindrance to the flow penetration and convection sinks more quickly which became less intense for higher Da values.

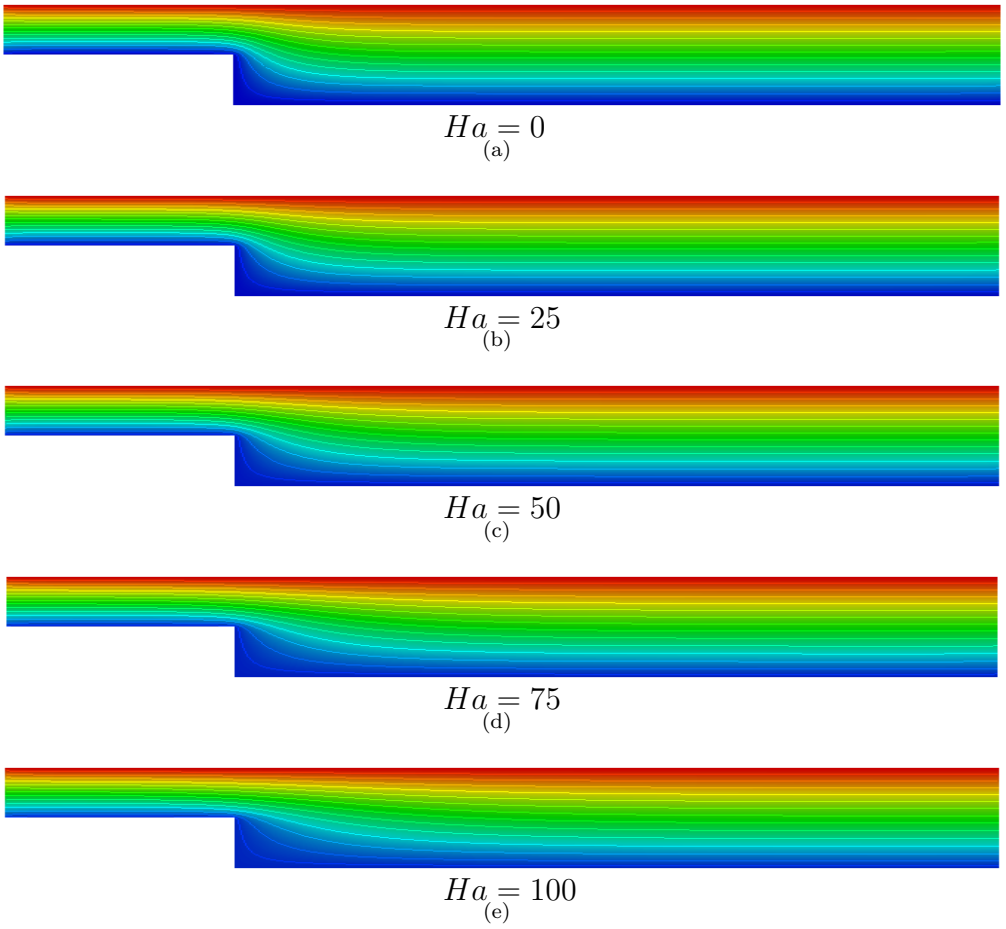

Figure 4.2: Streamlines for different Ha at $\gamma = 0^{\circ}$ and $\phi = 0.04$.

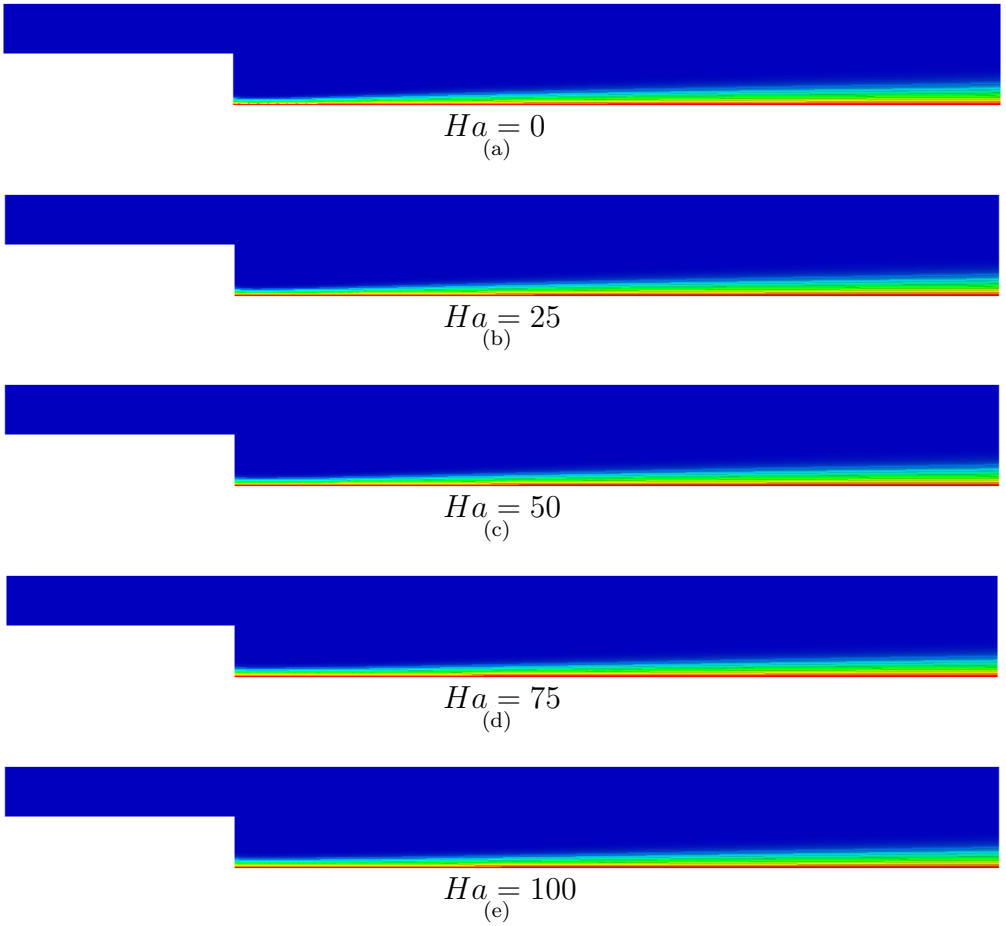

Figure 4.3: Isotherms for different Ha at $\gamma = 0^{\circ}$ and $\phi = 0.04$.

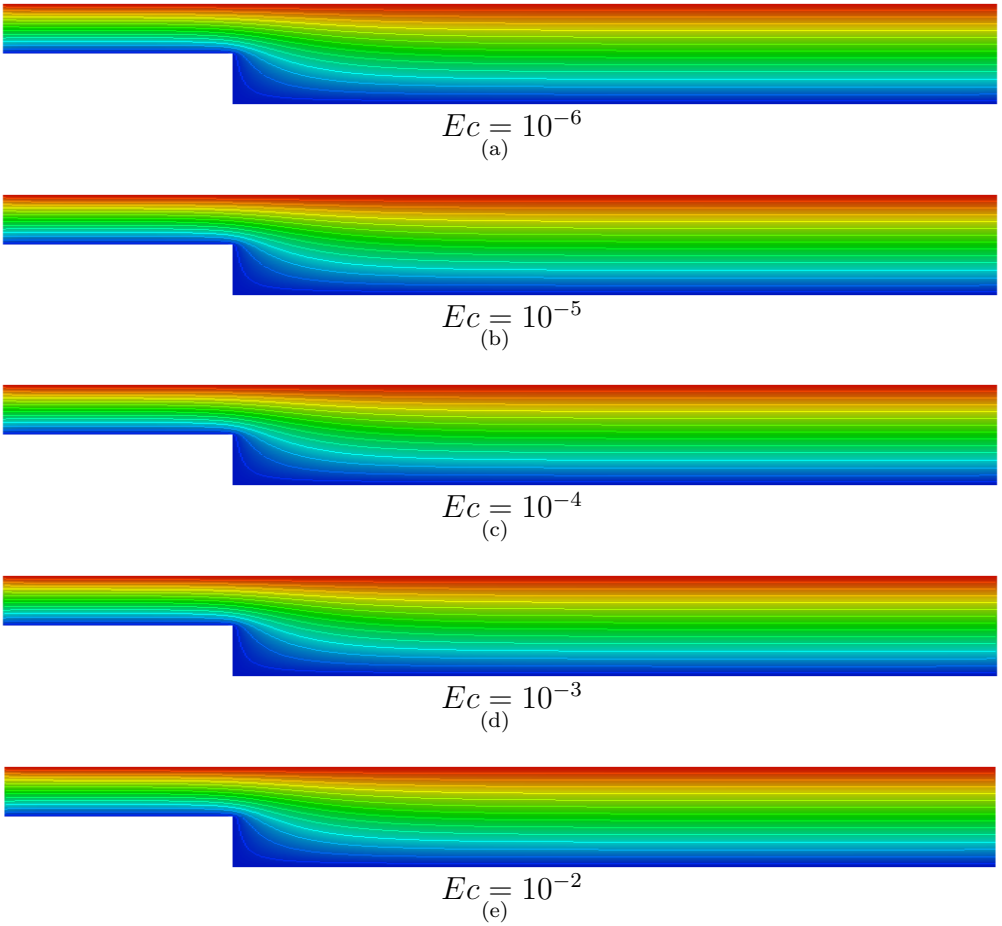

Figure 4.4: Streamlines for different Ec at $Ha = 100$, $\gamma = 0^{\circ}$ and $\epsilon = 1$.

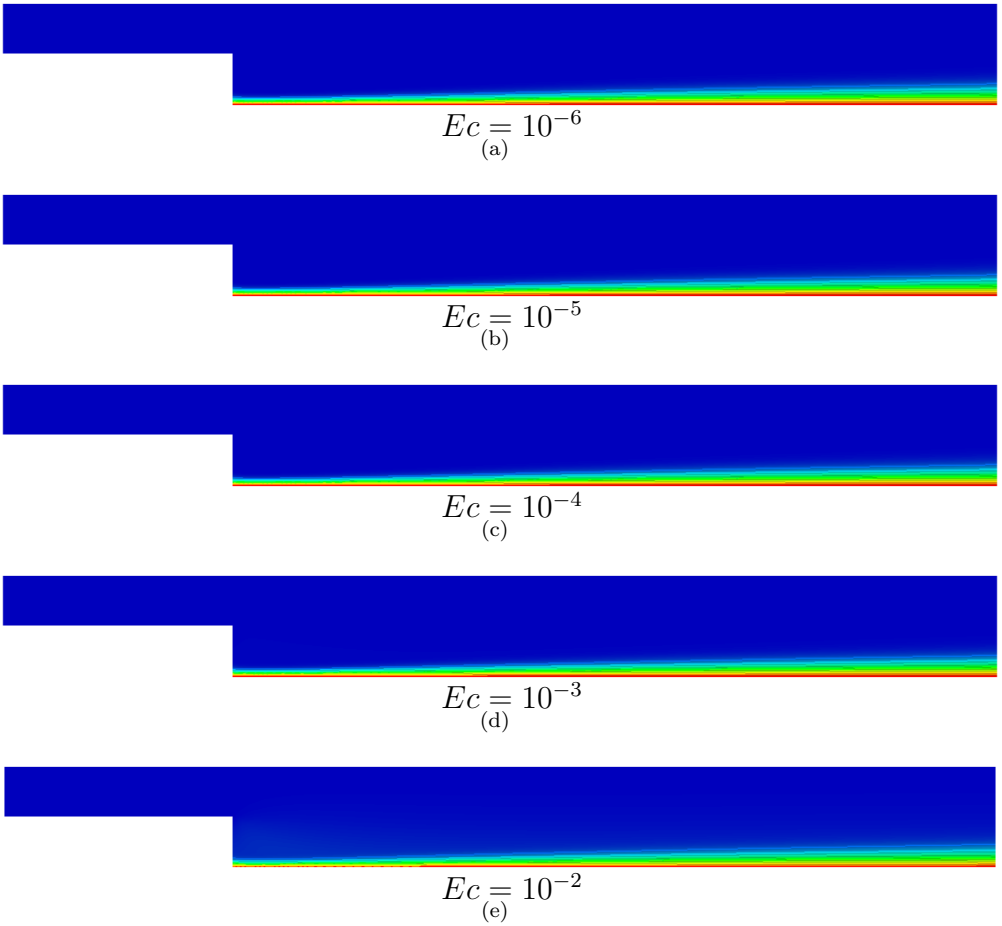

Figure 4.5: Isotherms for different Ec at $Ha = 100$, $\gamma = 0^{\circ}$ and $\epsilon = 1$.

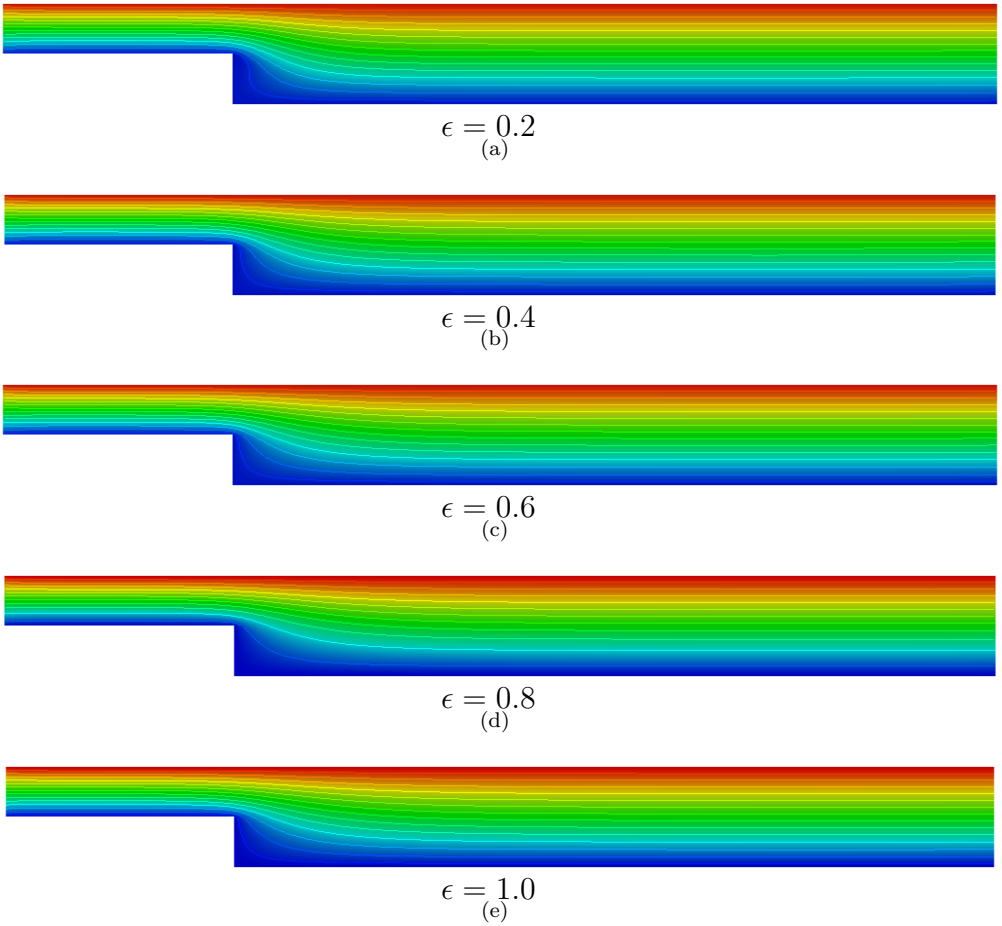

Figure 4.6: Streamlines for different ϵ at $Ec = 10^{-6}$, $Da = 10^{-3}$, $\phi = 0.04$ and $\gamma = 0^{\circ}$

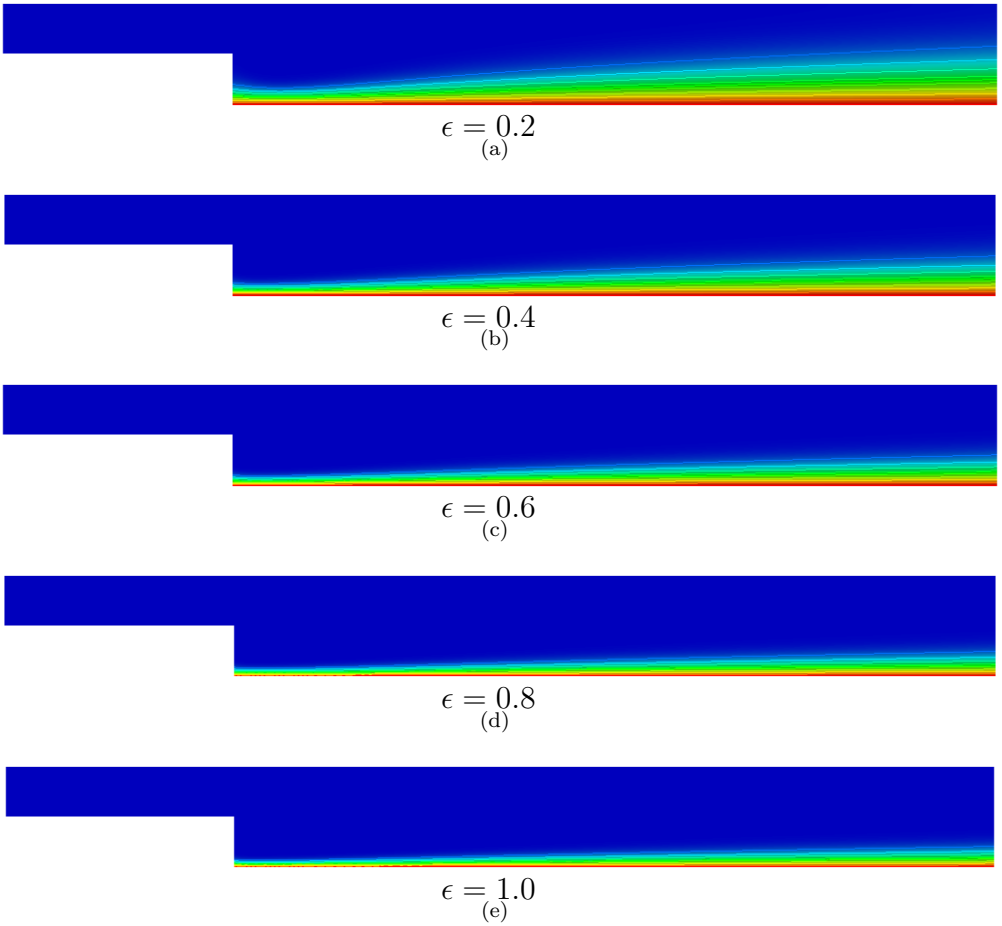

$\epsilon = 0.2$
(a)

$\epsilon = 0.4$
(b)

$\epsilon = 0.6$
(c)

$\epsilon = 0.8$
(d)

$\epsilon = 1.0$
(e)

Figure 4.7: Isotherms for different ϵ at $Ec = 10^{-6}$, $Da = 10^{-3}$, $\phi = 0.04$ and $\gamma = 0°$.

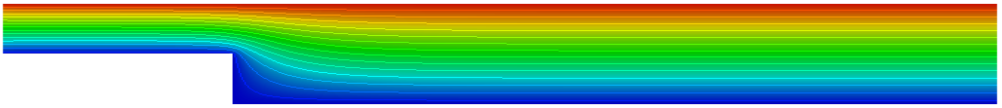

$Da = 10^{-4}$
(a)

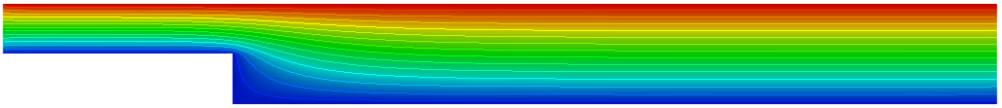

$Da = 10^{-3}$
(b)

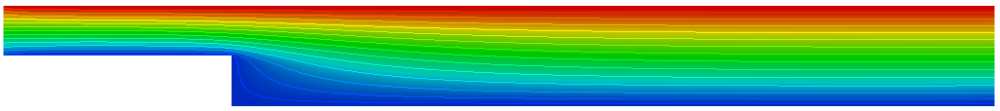

$Da = 10^{-2}$
(c)

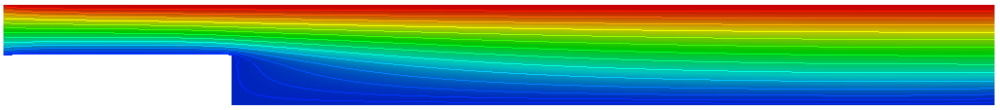

$Da = 10^{-1}$
(d)

Figure 4.8: Streamlines for different Da at $Ec = 10^{-6}$, $\epsilon = 1$, $\phi = 0.04$, and $\gamma = 0°$.

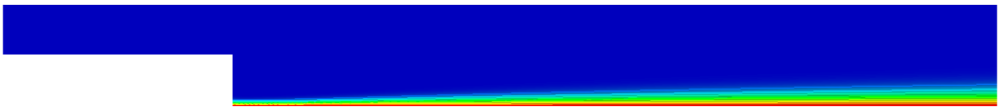

$Da = 10^{-4}$
(a)

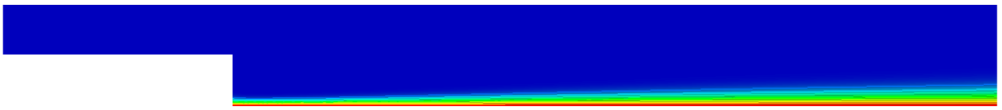

$Da = 10^{-3}$
(b)

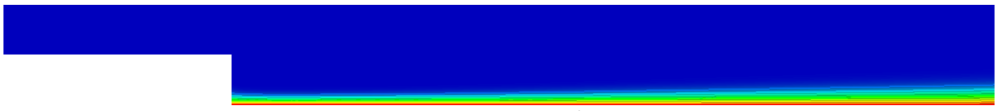

$Da = 10^{-2}$
(c)

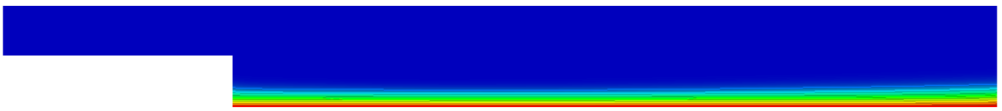

$Da = 10^{-1}$
(d)

Figure 4.9: Isotherms for different Da at $Ec = 10^{-6}$, $\epsilon = 1$, $\phi = 0.04$ and $\gamma = 0°$.

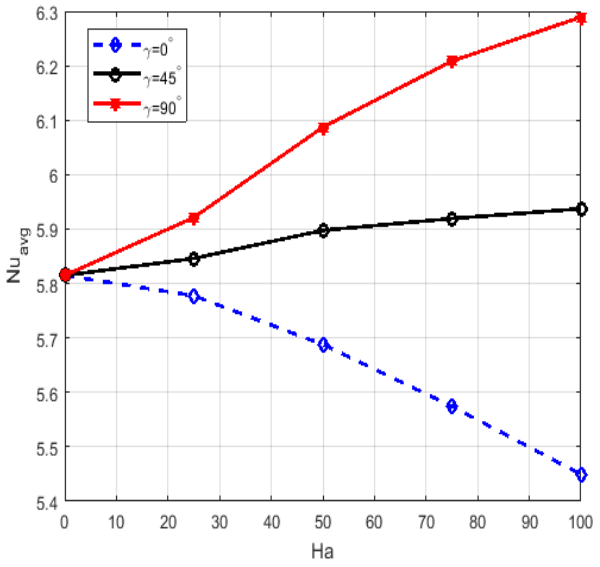

Figure 4.10: Variation of Nu_{avg} with increasing γ as a function of Ha.

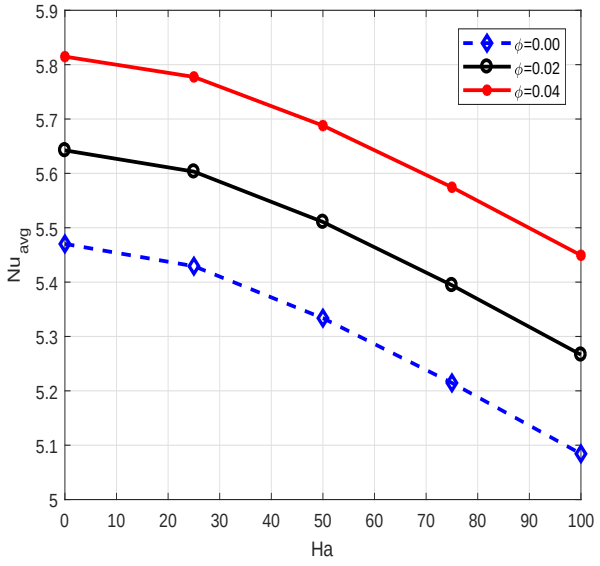

Figure 4.11: Variation of Nu_{avg} with increasing ϕ as a function of Ha.

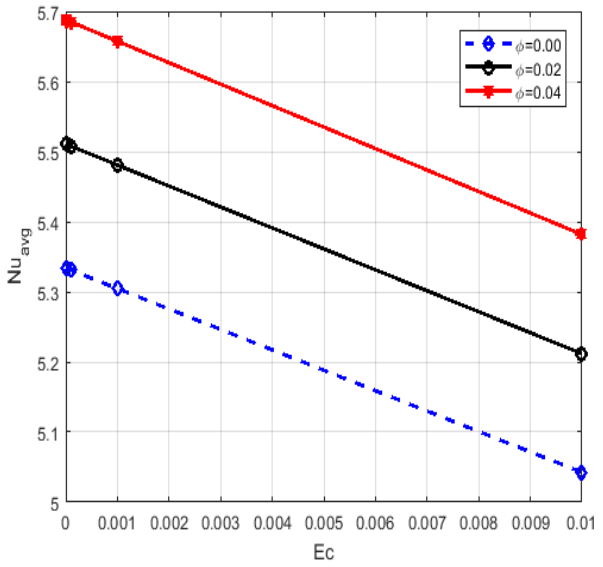

Figure 4.12: Variation of Nu_{avg} with increasing ϕ as a function of Ec.

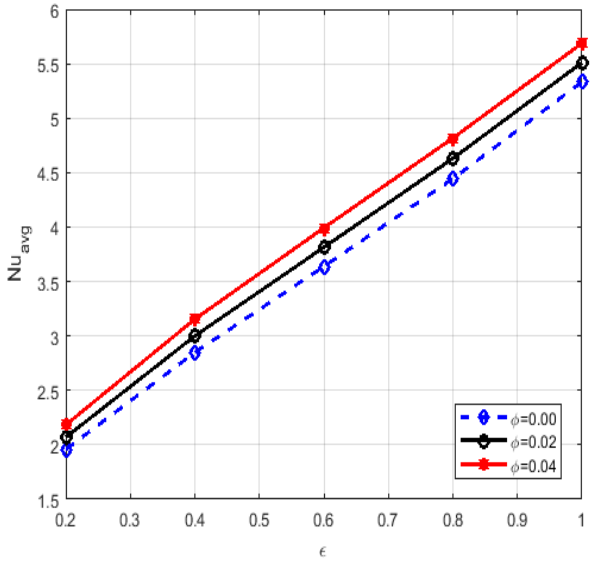

Figure 4.13: Variation of Nu_{avg} with ϕ as a function of ϵ.

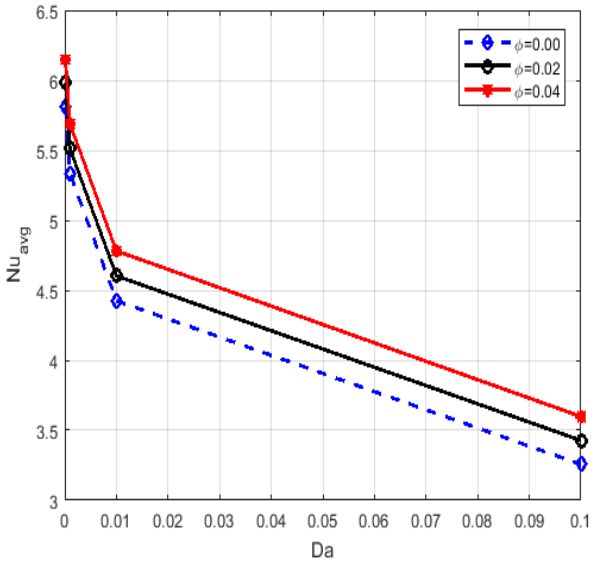

Figure 4.14: Variation of upon Nu_{avg} with ϕ as a function of Da.

Chapter 5

Closing Remarks

Present work is based on the investigation of a BFS channel filled with Cu-water nanofluid. Latterly, introduced with porous media and Joule heating effects under combined convection were reviewed. Horizontal wall of BFS is heated. Rest of the plates are thermally insulated. Transfer of heat by convection under later assumption were meditated. Governing equations of momentum and energy were furnished with the suitable terms and parameters, inducted with BDF model. Heat flow and thermal contouring were reviewed under the controlling parameters. Conclusive statements are created in the following manner.

The present body of research is made on the scholarly work of Selimefendigil and Öztop [1], extended by considering the porous medium and Joule heating effect in the present configuration. For this, state equations are modeled under DBF model for porous medium. Some important findings from the research conducted are as under:

- Thermal heat transfer is firmly depending on γ. For the amplifying γ with altering Ha, supremum heat transfer is accomplished at $\gamma = 90°$ for $Ha = 100$. Evidently, by increasing magnetic field inclination, a better convective heat transfer can be accomplished.

- Surely, magnetic field affected heat convection due to induced Lorentz forces for entire values of ϕ. Furthermore, after a certain $Ha = 25$ value as magnetic field strengthens, Nu_{avg} decays more quick.

- It is visible that Nusselt averaged is a lowering function of Ec in favour of ϕ. Increases Ec causing fluid to lose thermal energy resulting in reduction of Nu_{avg}.

- Nu_{avg} has dropped by rising Da values that proffer more declaration to fluid for higher Da values. Clearly, less permeability offers more hindrance, average Nusselt number decreases more quickly and more permeability gives less hindrance that is the reason after certain Da, average Nusselt number decreases less quickly.

- Seemingly, nanoparticle volume fraction has an impact on Nu_{avg} for greater porosity. As $\phi = 0.04$ has heightened the heat transfer rate by the reason of less recirculation and more fluid absorption.

Bibliography

[1] F. Selimefendigil and H. F. Öztop, "Influence of inclination angle of magnetic field on mixed convection of nanofluid flow over a backward facing step and entropy generation," *Advanced Powder Technology*, vol. 26, no. 6, pp. 1663–1675, 2015.

[2] K. Khanafer, B. Al-Azmi, A. Al-Shammari, and I. Pop, "Mixed convection analysis of laminar pulsating flow and heat transfer over a backward-facing step," *International Journal of Heat and Mass Transfer*, vol. 51, no. 25-26, pp. 5785–5793, 2008.

[3] J. Rajasekaran, *"On the flow characteristics behind a backward-facing step and the design of a new axisymmetric model for their study"*. University of Toronto, ON, Canada, 2011.

[4] E. Erturk, "Numerical solutions of 2D steady incompressible flow over a backward-facing step, part I: High reynolds number solutions," *Computers & Fluids*, vol. 37, no. 6, pp. 633–655, 2008.

[5] L. Chen, K. Asai, T. Nonomura, G. Xi, and T. Liu, "A review of backward-facing step BFS flow mechanisms, heat transfer and control," *Thermal Science and Engineering Progress*, vol. 6, pp. 194–216, 2018.

[6] A. Al-Aswadi, H. Mohammed, N. Shuaib, and A. Campo, "Laminar forced convection flow over a backward facing step using nanofluids," *International Communications in Heat and Mass Transfer*, vol. 37, no. 8, pp. 950–957, 2010.

[7] H. Iwai, K. Nakabe, and K. Suzuki, "Flow and heat transfer characteristics of backward-facing step laminar flow in a rectangular duct," *International Journal of Heat and Mass Transfer*, vol. 43, no. 3, pp. 457–471, 2000.

[8] J. Nie and B. F. Armaly, "Convection in laminar three dimensional separated flow," *International Journal of Heat and Mass Transfer*, vol. 47, no. 25, pp. 5407–5416, 2004.

[9] B. F. Armaly, F. Durst, J. Pereira, and B. Schönung, "Experimental and theoretical investigation of backward-facing step flow," *Journal of Fluid Mechanics*, vol. 127, pp. 473–496, 1983.

[10] S. K. Das, S. U. Choi, and H. E. Patel, "Heat transfer in nanofluids a review," *Heat Transfer Engineering*, vol. 27, no. 10, pp. 3–19, 2006.

[11] S. T. Picraux, "Nanotechnology," *Encyclopædia Britannica, inc.*, p. 1, 2018.

[12] S. Choi, "Enhancing thermal conductivity of fluids with nanoparticles," *ASME International Mechanical Engineering Congress amd Exposition*, vol. 231, pp. 99–103, 1995.

[13] S. Mukherjee and S. Paria, "Preparation and stability of nanofluids-a review," *IOSR Journal of Mechanical and Civil Engineering*, vol. 9, no. 2, pp. 63–69, 2013.

[14] R. Pal, "A novel method to determine the thermal conductivity of interfacial layers surrounding the nanoparticles of a nanofluid," *Nanomaterials*, vol. 4, no. 4, pp. 844–855, 2014.

[15] S. Choi, "Nanofluids: A new field of scientific research and innovative applications," *Heat Transfer Engineering*, vol. 29, no. 5, pp. 429–431, 2008.

[16] W. Yu and H. Xie, "A review on nanofluids: preparation, stability mechanisms, and applications," *Journal of Nanomaterials*, vol. 2012, p. 1, 2012.

[17] D. K. Devendiran and V. A. Amirtham, "A review on preparation, characterization, properties and applications of nanofluids," *Renewable and Sustainable Energy Reviews*, vol. 60, pp. 21–40, 2016.

[18] F. Selimefendigil and H. F. Öztop, "Numerical investigation and reduced order model of mixed convection at a backward facing step with a rotating cylinder subjected to nanofluid," *Computers & Fluids*, vol. 109, pp. 27–37, 2015.

[19] E. Abu-Nada, "Application of nanofluids for heat transfer enhancement of separated flows encountered in a backward facing step," *International Journal of Heat and Fluid Flow*, vol. 29, no. 1, pp. 242–249, 2008.

[20] X. Q. Wang and A. S. Mujumdar, "Heat transfer characteristics of nanofluids: a review," *International Journal of Thermal Sciences*, vol. 46, no. 1, pp. 1–19, 2007.

[21] V. Trisaksri and S. Wongwises, "Critical review of heat transfer characteristics of nanofluids," *Renewable and Sustainable Energy Reviews*, vol. 11, no. 3, pp. 512–523, 2007.

[22] O. Mahian, A. Kianifar, S. A. Kalogirou, I. Pop, and S. Wongwises, "A review of the applications of nanofluids in solar energy," *International Journal of Heat and Mass Transfer*, vol. 57, no. 2, pp. 582–594, 2013.

[23] D. Wen and Y. Ding, "Formulation of nanofluids for natural convective heat transfer applications," *International Journal of Heat and Fluid Flow*, vol. 26, no. 6, pp. 855–864, 2005.

[24] J. Kestin and W. Wakeham, "A contribution to the theory of the transient hot-wire technique for thermal conductivity measurements," *Physica A: Statistical Mechanics and its Applications*, vol. 92, no. 1-2, pp. 102–116, 1978.

[25] Y. Nagasaka and A. Nagashima, "Absolute measurement of the thermal conductivity of electrically conducting liquids by the transient hot-wire method," *Journal of Physics E: Scientific Instruments*, vol. 14, no. 12, p. 1435, 1981.

[26] J. P. Hartnett, W. M. Rohsenow, E. Ganic, and Y. Cho, *Handbook of Heat Transfer*. Mc Graw Hill, 1973.

[27] R. Patra, S. Das, and R. N. Jana, "Radiation effect on MHD fully developed mixed convection in a vertical channel with asymmetric heating," *Journal of Applied Fluid Mechanics*, vol. 7, no. 3, pp. 503–512, 2014.

[28] I. Arroub, A. Bahlaoui, A. Raji, M. Hasnaoui, and M. Naïmi, "Varying heating effect on mixed convection of nanofluids in a vented horizontal cavity with injection or suction," *Heat Transfer Engineering*, vol. 40, no. 11, pp. 941–958, 2019.

[29] J. Saldana, N. Anand, and V. Sarin, "Numerical simulation of mixed convective flow over a three-dimensional horizontal backward facing step," *Journal of Heat Transfer*, vol. 127, no. 9, pp. 1027–1036, 2005.

[30] H. Abu-Mulaweh, "A review of research on laminar mixed convection flow over backward and forward-facing steps," *International Journal of Thermal Sciences*, vol. 42, no. 9, pp. 897–909, 2003.

[31] F. Selimefendigil and H. F. Öztop, "Identification of forced convection in pulsating flow at a backward facing step with a stationary cylinder subjected to nanofluid," *International Communications in Heat and Mass Transfer*, vol. 45, pp. 111–121, 2013.

[32] A. Kumar and A. K. Dhiman, "Effect of a circular cylinder on separated forced convection at a backward-facing step," *International Journal of Thermal Sciences*, vol. 52, pp. 176–185, 2012.

[33] M. Sheikholeslami and D. Ganji, *Magnetohydrodynamic and Ferrohydrodynamic*. Elsevier, 12 2016, pp. 1–47.

[34] N. Bakar, A. Karimipour, and R. Roslan, "Effect of magnetic field on mixed convection heat transfer in a lid-driven square cavity," *Journal of Thermodynamics*, vol. 2016, 2016.

[35] H. Abbassi and S. B. Nassrallah, "MHD flow and heat transfer in a backward-facing step," *International communications in heat and mass transfer*, vol. 34, no. 2, pp. 231–237, 2007.

[36] A. S. Kherbeet, H. Mohammed, and B. Salman, "The effect of nanofluids flow on mixed convection heat transfer over microscale backward-facing step," *International Journal of Heat and Mass Transfer*, vol. 55, no. 21-22, pp. 5870–5881, 2012.

[37] A. S. Kherbeet, H. Mohammed, B. Salman, H. E. Ahmed, O. A. Alawi, and M. Rashidi, "Experimental study of nanofluid flow and heat transfer over microscale backward-and forward-facing steps," *Experimental Thermal and Fluid Science*, vol. 65, pp. 13–21, 2015.

[38] F. Selimefendigil and H. F. Oztop, "Control of laminar pulsating flow and heat transfer in backward-facing step by using a square obstacle," *Journal of Heat Transfer*, vol. 136, no. 8, p. 081701, 2014.

[39] F. Selimefendigil and H. F. Öztop, "Laminar convective nanofluid flow over a backward-facing step with an elastic bottom wall," *Journal of Thermal Science and Engineering Applications*, vol. 10, no. 4, p. 041003, 2018.

[40] S. Hussain, K. Mehmood, M. Sagheer, and A. Farooq, "Entropy generation analysis of mixed convective flow in an inclined channel with cavity with al2o3-water nanofluid in porous medium," *International Communications in Heat and Mass Transfer*, vol. 89, pp. 198–210, 2017.

[41] S. Hussain, K. Mehmood, M. Sagheer, and A. Ashraf, "Mixed convective magnetonanofluid flow over a backward facing step and entropy generation using extended darcy–brinkman–forchheimer model," *Journal of Thermal Analysis and Calorimetry*, pp. 1–21, 2019.

[42] S. Hassanizadeh, *Theory and Applications of Transport in Porous Media*. Springer International Publishing, 2019, vol. 32.

[43] K. M. Khanafer and A. J. Chamkha, "Mixed convection flow in a lid-driven enclosure filled with a fluid-saturated porous medium," *International Journal of Heat and Mass Transfer*, vol. 42, pp. 2465–2481, 1999.

[44] A. A. Hassan and M. A. Ismael, "Mixed convection in superposed nanofluid and porous layers inside lid-driven square cavity," *International Journal of Thermal & Environmental Engineering*, vol. 10, no. 2, pp. 93–104, 2015.

[45] A. C. Yunus, *Fluid Mechanics: Fundamentals And Applications.* Tata Mc Graw Hill Education Private Limited, 2006.

[46] F. M. White, *Fluid Mechanics.* Mc Graw Hill, 2011.

[47] A. C. Yunus, *Fluid Mechanics: Fundamentals And Applications.* Tata Mc Graw Hill Education Private Limited, 2014.

[48] ——, *Fluid Mechanics: Fundamentals And Applications (Si Units).* Tata Mc Graw Hill Education Private Limited, 2010.

[49] S. K. Das, S. U. Choi, W. Yu, and T. Pradeep, *Nanofluids: Science And Technology.* John Wiley & Sons, 2007.

[50] N. Singh, *Fluid Mechanics.* Random Publications, 2014.

[51] G. Sawhney, *Fundamentals of Fluid Mechanics, Second Edition.* I.K. International Publishing House Private Limited, 2013.

[52] M. Raisinghania, *Fluid Dynamics.* S. Chand Publishing, 2003.

[53] H. K. Versteeg and W. Malalasekera, *An Introduction to Computational Fluid Dynamics: the Finite Volume Method.* Pearson Education, 2007.

[54] J. Kunes, *Dimensionless Physical Quantities in Science and Engineering.* Elsevier, 2012.

[55] F. M. White, "Fluid mechanics," *Mc Graw Hill, New York, NY*, vol. 10020, pp. 366–376, 2003.

[56] P. Papadopoulos, "Introduction to the finite element method," *California: Berkeley University of California*, 2010.

[57] D. L. Logan, *A First Course in the Finite Element Method.* Cengage Learning, 2011.

[58] D. M. Driver and H. L. Seegmiller, "Features of a reattaching turbulent shear layer in divergent channel flow," *AIAA Journal*, vol. 23, no. 2, pp. 163–171, 1985.

[59] A. H. Mahmoudi, I. Pop, and M. Shahi, "Effect of magnetic field on natural convection in a triangular enclosure filled with nanofluid," *International Journal of Thermal Sciences*, vol. 59, pp. 126–140, 2012.

[60] Z. Mehrez, A. El Cafsi, A. Belghith, and P. Le Quéré, "MHD effects on heat transfer and entropy generation of nanofluid flow in an open cavity," *Journal of Magnetism and Magnetic Materials*, vol. 374, pp. 214–224, 2015.

[61] B. S. Alshuraiaan, "Mixed convection flow and heat transfer over different geometries of backward-facing step," *Journel of Engineering Research*, vol. 1, pp. 211–233, 2013.

[62] Q. H. S. Acharya, G. Dixit, "Laminar mixed convection in a vertical channel with a backstep: a benchmark study," *ASME HTD*, vol. 258, pp. 11–20, 1993.

[63] T. C. J. Lin, B. Armaly, "Mixed convection in buoyancy-assisted vertical backward-facing step flows," *International Journal Heat Mass Transfer*, vol. 33, pp. 2121–2132, 1990.

[64] D. S. Cimpean and I. Pop, "Fully developed mixed convection flow of a nanofluid through an inclined channel filled with a porous medium," *International Journal of Heat and Mass Transfer*, vol. 55, no. 4, pp. 907–914, 2012.

[65] M. Sheikholeslami, M. G. Bandpy, R. Ellahi, and A. Zeeshan, "Simulation of mhd cuo-water nanofluid flow and convective heat transfer considering lorentz forces," *Journal of Magnetism and Magnetic Materials*, vol. 369, pp. 69–80, 2014.

[66] M. Sheikholeslami, K. Vajravelu, and M. M. Rashidi, "Forced convection heat transfer in a semi annulus under the influence of a variable magnetic field," *International Journal of heat and Mass Transfer*, vol. 92, pp. 339–348, 2016.

[67] K. Mehmood, S. Hussain, and A. Sagheer, "Entropy generation analysis of mixed convective flow in an inclined channel with cavity with al_2o_3-water nanofluid in porous medium," *International Communications in Heat and Mass Transfer*, vol. 89, pp. 198–210, 2017.